

# **Mantle heterogeneities produced by open-system melting and melt/rock reactions in Patagonian extra-Andean backarc mantle (Paso de Indios, Argentina)**

Gustavo W. Bertotto<sup>1</sup>, Maurizio Mazzucchelli<sup>2,3</sup>, Alberto Zanetti<sup>3</sup>, Alexis D. Ponce<sup>1</sup>, Tommaso Giovanardi<sup>2\*</sup>, Daniele Brunelli<sup>2,4</sup>, Mauro I. Bernardi<sup>1</sup>, Christophe Hémond<sup>5</sup>, Anna Cipriani<sup>2,6</sup>

<sup>1</sup> CONICET-Universidad Nacional de La Pampa, Instituto de Ciencias de la Tierra y Ambientales de La Pampa (INCITAP), Uruguay 151, 6300, Santa Rosa, Argentina.

<sup>2</sup> Dipartimento di Scienze Chimiche e Geologiche, Università degli Studi di Modena e Reggio Emilia, Via Campi 103, I-41125, Modena, Italy.

<sup>3</sup> Istituto di Geoscienze e Georisorse - CNR, U.O.S. di Pavia, Via Ferrata 1, I-27100 Pavia, Italy.

<sup>4</sup> Istituto di Scienze del Mare, ISMAR CNR, Via Gobetti 101, I-41100, Bologna, Italy.

<sup>5</sup> Laboratoire Géosciences Océan, UMR6538, Institut Universitaire Européen de la Mer, Université de Brest & CNRS, Place Nicolas Copernic, F-29280, Plouzané, France.

<sup>6</sup> Lamont-Doherty Earth Observatory of Columbia University, 61 Route 9W, Palisades NY 10964-1000 USA

Corresponding email: tommaso.giovanardi@gmail.com

Keywords: Patagonia, Mantle xenoliths, Mantle melting, Mantle metasomatism

## **ABSTRACT**

The Eocene basaltic extrusions in the Paso de Indios region (Chubut-Argentina) are one manifestation of the extensional tectonism of the active margin of South America during the Cenozoic. Ultramafic xenoliths embedded in these volcanics are mainly harzburgites and lherzolites with subordinate pyroxenites, estimated equilibrium temperatures ranging from  $853 \pm 15$  to  $1057 \pm 32^\circ\text{C}$  and pressures in the spinel stability field.

Geochemical and modal evidences point to a multistage magmatic history with record of a last reactional open-system episode associated to the influx of adakitic-like melts in a orthopyroxene-rich, clinopyroxene-poor mantle column. The great variability of clinopyroxene modal and geochemical composition in a  $\sim 20 \text{ km}^2$  area suggests extreme variability of the physical parameters connected to melt infiltration and melt/rock reactions

Formatted: English (United States)

processes at a very small scale superimposed on a mantle with an inherited meter scale heterogeneity. Variations in the melt influx rate and residual porosity of the mantle column produced different melt/rock reactions which could be summarized in two entangled main reaction pathways: 1)  $\text{opx} + \text{cpx} + \text{melt1} \rightarrow \text{ol} + \text{melt2}$  and 2)  $\text{opx} + \text{melt1} \rightarrow \text{cpx} + \text{ol} + \text{melt2}$ . These reactions deeply modified the trace elements content of clinopyroxenes producing variable enrichments in LREEs and LILEs related to both chromatographic and pure incremental open system processes.

Petrological evidence suggests that the last reactional process occurred in the spinel stability field overprinting a strongly depleted mantle that, in a previous stage, had experienced extreme depletion in the garnet stability field, possibly under hydrous conditions.

The adakitic-like nature of the influxing melt associates this episode to the subduction system along the western margin of South America, active at least since Late Triassic times.

## 1. Introduction

The South American sublithospheric mantle records a complex sequence of depletion and refertilization episodes linked to the geodynamic evolution of supercontinents and large igneous provinces (e.g. Mazzucchelli et al., 1995, 2016; Rivalenti et al., 1995, 2004a, 2007a, 2007b; Correia et al., 2012; Faccini et al., 2013; Giovanardi et al., 2018, 2019; Roverato et al., 2019; Liu et al., 2019a; 2019b; Melchiorre et al., 2020). In this context, Patagonia (southern Argentina,  $\sim 38^{\circ}$ - $53^{\circ}$ S) is a relatively large area, comprising part of the back-arc region of the Andean arc, in which Pliocene-Quaternary alkaline basalt volcanism is randomly distributed (Stern et al., 1990). Mantle xenoliths from more than twenty well known of these basaltic outcrops, record geochemical evidence of depletion, metasomatism and refertilization processes related to the influence of the subduction system active at least since the Triassic along the western border of South America (Melchiorre et al., 2020 and references therein).

The very first Patagonian mantle xenoliths ever studied were from the localities of Comallo and Los Adobes in the North (Gelós and Hayase, 1979). Decades later, mantle xenoliths collected and studied from the entire Patagonia, from the Payenia region in the North to the Tierra del Fuego to the South, were found to be mainly equilibrated in the spinel stability field (Bjerg et al., 1991, 2005; Barbieri et al., 1999; Bertotto, 2000; Acevedo and Quartino, 2004; Rivalenti et al., 2004a; Jalowitzki et al., 2010; Bertotto et al., 2013; Mazzucchelli et al., 2016; Melchiorre et al., 2020). Garnet-bearing peridotites were identified only in Prahuaní in northern Patagonia (Ntaflos et al., 2001; Ntaflos and Bjerg, 2006; Bjerg et

al., 2009) and in Pali Aike, in the **S**outh (Skewes and Stern, 1979; Douglas et al., 1987; Kempton et al., 1999; Vannucci et al., 2002; Zaffarana et al., 2014).

In the area of Paso de Indios (PDI, northern Patagonia), several outcrops of Paleogene basalts known as Cerro León, Cerro Matilde and Cerro Chenque (hereafter named León, Matilde and Chenque) contain strongly heterogeneous mantle xenoliths in the spinel facies (Gelós and Hayase, 1979; Alric et al., 1993; Labudía, 1994; Alric, 1996 Rivalenti et al. (2004a) with HREE in clinopyroxene that suggest enhanced partial melting depletion (Rivalenti et al., 2004a; this work). This is a unique case in the Patagonia region, where the mantle column is generally completely overprinted by melt intrusions and refertilization events (Bjerg et al., 1991, 2005; Barbieri et al., 1999; Bertotto, 2000; Acevedo and Quartino, 2004; Rivalenti et al., 2004a; Jalowitzki et al., 2010; Bertotto et al., 2013; Mazzucchelli et al., 2016; Melchiorre et al., 2020). A few granulitic xenoliths found in Chenque were interpreted as solid residues after separation of granitic to granodioritic melts (Castro et al., 2011). A zircon U-Pb age dates this event at  $175.9 \pm 4.9$  Ma during a time of complex lithospheric evolution for Patagonia in a geodynamic context preceding the rupture of Gondwana.

In spite of all these studies, the reported petrochemical information is insufficient to characterize in detail the composition of the lithospheric mantle and the associated petrological processes that affected the PDI mantle column. This is due to the low number of samples and the fact that, among the several outcrops of the area, the studied xenoliths are mainly from Chenque (Rivalenti et al., 2004; Bjerg et al., 2005). A more recent petrological study, based on the major element composition of mineral phases of xenoliths from all three basaltic outcrops in the PDI area has shown more variable geochemical and petrological features than previously reported (Ponce et al., 2015). We have increased the number of xenoliths studied in this area and analyzed the trace element composition of clinopyroxenes from the xenoliths of Ponce et al (2015) and new xenoliths of this collection. Combining new and old petrographic observations and major elements analyses with our complete trace element dataset, we discuss evidence supporting open system partial melting processes as responsible for the petrochemical characteristics of the mantle column below the PDI area.

## **2. Geological background**

The study area is located in the extra-Andean zone of north Patagonia near the town of Paso de Indios (PDI, Chubut province, Argentina) (Fig. 1) and is part of the geological province of the Patagónides (Ramos, 1999; Giacosa and Márquez, 1999). In this area, ultramafic

xenoliths have been reported in eight basaltic outcrops (Alric, 1996) and belong to the El Buitre Formation (Ardolino and Franchi, 1993). We analyzed samples from three relicts of Eocene lava flows and dykes with alkaline composition, namely Matilde, León and Chenque (Fig. 1). These basalts cover and intrude Cretaceous sedimentary rocks and are partially covered by Quaternary debris (Alric et al., 2002; Anselmi et al., 2004; Silva Nieto, 2005). They are related to the Paleogene Rift of the Patagónides (Aragón et al., 2015), which formed when extensional tectonics affected the active margin of southern South America from the Paleocene to the Oligocene. This extensional event was triggered by the arrival of the transform plate boundary at the subduction zone, with the tearing of the Farallón-Aluk plate triggering the formation of a slab window (Aragón et al., 2011).

Chenque is a basaltic dyke, about 50 meters long, located at 68°56'37" W and 43°38'37" S with an estimated age of 52 Ma based on the geochemical affinity with similar basaltic dykes of the region (Alric et al., 2002). Matilde is a remnant of a lava flow at 68°55'27" W and 43°48'42" S with an Ar-Ar age of  $49.35 \pm 0.74$  Ma (Alric, 1996). Lastly, León, partly covered by basaltic debris and recent sediments, is 50.17 Ma old ( $\pm 0.41$ ; Alric, 1996) and located at 69°0'14" W and 43°42'9" S (Fig. 1).

### 3. Analytical methods

In this work, we discuss new chemical data of eighteen samples (12 from Chenque, 2 from Matilde and 4 from León) together with eleven samples (5 from Chenque, 5 from Matilde and 1 from León) previously analyzed for major elements only (Ponce et al., 2015). Modes are reported in Table 1.

As discussed below, the occurrence within the xenoliths of glass veins from the host basalt has produced strong reaction at the contact with the mineral phases. However, given that our aim is to reconstruct the composition and characteristics of the original mantle column beneath the PDI area, all our data have been collected at the mineral core. Similar studies have already demonstrated that the reaction of minerals with host basalt affected their composition only at the rim thus preserving their original composition in the cores (e.g. Laurora et al., 2001).

Whole rock major and trace element were analyzed by inductively coupled plasma atomic emission spectrometry (ICP-AES) at the "Université de Bretagne Occidentale" (Brest, France) following methods described in Cotten et al. (1995). To remove alteration effects, the whole-rock powders were leached with 2.5N HCl for 10 min in an ultrasonic bath and rinsed three times in ultrapure water. Relative standard deviations were <2% for major

elements, Rb and Sr and <5% for the other trace elements. Data are reported in Supplementary Material 1, Table 1.

Major elements in mineral phases were determined at the Dipartimento di Scienze della Terra of the Università di Milano (Italy) with a JEOL JXA-8200 electron microprobe using a 15 kV accelerating voltage, 15 nA beam current, 1-3  $\mu\text{m}$  beam diameter, 30 s counting time on the peaks and 10 s on the background. Natural minerals (olivine for Mg; omphacite for Na; ilmenite for Ti; rodonite for Mn; K-feldspar for K; anorthite for Al and Ca; wollastonite for Si; fayalite for Fe and nicolite for Ni) and synthetic chromite were used as standards. The results were corrected for matrix effects using the conventional ZAF method provided by the JEOL suite of programs. Results are considered to be accurate within 2-6%. Details on the methodology are reported in Giovanardi et al. (2020). Averages of each sample are presented in Tables 2-5 and the entire dataset is reported in Supplementary Material 2.

Trace-elements in clinopyroxene and orthopyroxene have been analyzed at Consiglio Nazionale delle Ricerche - Istituto di Geoscienze e Georisorse (Section of Pavia, Italy) by laser ablation-inductively coupled plasma-mass spectrometry (LA-ICP-MS) using a Perkin Elmer ELAN DRC-e quadrupole mass spectrometer coupled with a Q-switched Nd:YAG laser source Brilliant, whose fundamental emission in the infrared region (1064 nm) is converted into 266 nm by two harmonic generators. The laser was operated at a repetition rate of 10 Hz, with a pulse energy of ~35 mJ. Helium was used as carrier gas and was mixed with Ar downstream of the ablation cell. Spot diameter was adjusted in the range of 40-80  $\mu\text{m}$ . Data reduction was performed offline using the GLITTER software. For this study, the NIST SRM 610 synthetic glass reference material was used as external standard and CaO was used as internal standard for clinopyroxene. Precision and accuracy of the REE concentration values were assessed through repeated analysis of the BCR2-g standard to be better than  $\pm 7\%$  and  $\pm 10\%$ , respectively at the ppm concentration level (further details are reported in Zanetti et al., 2016). Average of each sample is reported in Table 6. The entire dataset is reported in Supplementary Material 3.

#### 4. Petrography

The studied xenoliths are anhydrous spinel-facies peridotites and pyroxenites. Based on modal analyses (by count pointing, at least 600 points for each sample) they can be classified as lherzolite (13 samples), harzburgite (12 samples), websterite (3 samples) and olivine-websterite (1 sample) (Fig. 2; Table 1). The predominant texture (after Harte, 1977) is

171 porphyroclastic, followed by the transitional coarse to porphyroclastic texture and, to a lesser  
172 extent, the coarse and mosaic-porphyroclastic textures (Fig. 3A-D). Among the three  
173 outcrops, Matilde xenoliths seem to be the most depleted, represented by harzburgites (five  
174 samples) and lherzolites (two samples; Fig. 2). León xenoliths comprise lherzolites (two  
175 samples), harzburgites (two samples) and one olivine-websterite (Fig. 2; Table 1). Xenoliths  
176 from Chenque show the highest modal variability with lherzolites (nine samples),  
177 harzburgites (five samples) and three websterites (Fig. 2; Table 1). Considering the modal  
178 variability of the PDI xenoliths (Fig. 2B), peridotites with low olivine are orthopyroxene-  
179 rich and clinopyroxene-poor compared to the modal composition of the primitive mantle  
180 (PM, Warren, 2016;). We now briefly synthesize the petrographic characteristics of the  
181 studied xenoliths, given that all details can be found in Ponce et al. (2015).

182 Olivine is present as large, mainly anhedral crystals up to 12 mm in length and small anhedral  
183 to subhedral crystals up to 0.5-2 mm. The larger olivines are kink-banded and the smaller  
184 are unstrained. Frequently, in samples of León and rarely in Matilde and Chenque, grains of  
185 1-2 mm of unstrained olivine occupy embayments of large orthopyroxene suggesting  
186 replacement (Fig. 3E).

187 Orthopyroxene is anhedral and up to 12 mm in diameter. Large grains commonly show a  
188 thin regular pattern of clinopyroxene exsolution lamellae and rarely kink-bands less  
189 developed than those of olivine. Vermicular orthopyroxene, sometimes associated with  
190 clinopyroxene and rarely with small and unstrained olivine, frequently replaces large  
191 strained olivine (Fig. 3F). Orthopyroxene shows partial to total replacement when in contact  
192 with the host lava by clinopyroxene + olivine + glass  $\pm$  orthopyroxene  $\pm$  spinel group  
193 minerals  $\pm$  plagioclase (Fig. 3G). Within the xenolith, orthopyroxene can develop reaction  
194 rims linked to veins of altered glass directly connected to the host basalt similar to what  
195 reported above.

196 Clinopyroxene is anhedral, reaching up to 3 mm in diameter. Rarely, clinopyroxene has  
197 cloudy appearance because of the occurrence of minute ( $<30\ \mu\text{m}$  diameter) melt inclusions.  
198 In olivine-rich harzburgites, clinopyroxene is interstitial, and sometimes is associated with  
199 secondary olivine replacing primary orthopyroxene. Rarely, clinopyroxene shows spongy  
200 rims with the development of a corona frequently linked to veins from the host basalt.

201 Spinel is mainly anhedral and reaches 2.7 mm in size. Holly-leaf shaped spinel is the most  
202 common and frequently observed in the porphyroclastic samples. Less frequently subhedral  
203 and euhedral spinels are included in olivine and are also present as rounded grains associated  
204 with secondary olivine and clinopyroxene replacing larger, primary orthopyroxenes.

Spinel+ol±opx irregular symplectites could represent garnet breakdown (Supplementary Material 4, Fig. 14) but according to Seyler et al. (2007) similar symplectites could also originate from melt reaction percolation in the spinel facies. As shown in Ponce et al. (2015), frequently the xenoliths bear veinlets of altered (serpentinized) glass from the host basalt.

## 5. Whole rock chemistry

Five whole rock analyzes were obtained from the core portion (2-3 cm in diameter) of xenolith samples larger than 10 cm. The abundance of MgO ranges between 42.6 and 44.0 wt.%. The compositional variation of MgO is within the range of those xenoliths previously reported for Patagonia (Rivalenti et al., 2004a, 2004b; Bjerg et al., 2005) and MgO shows a negative correlation with Al<sub>2</sub>O<sub>3</sub>, CaO, TiO<sub>2</sub> and Na<sub>2</sub>O content (Supplementary Material 1, Fig. 1). As a whole, PDI harzburgites and lherzolites are, on average, between the more refractory spinel facies xenoliths from South America (Rivalenti et al., 2004a, 2004b; Bjerg et al., 2005; Ntaflou et al., 2007). Further discussion about whole rock data can be misleading because of the disturbing influence of intergranular glass films or veins (see Supplementary Material 1 and 4, Table 1). The infiltrating melt shows strong reactivity with the xenoliths minerals as suggested by the extreme variability in the chemical composition of the veins (Supplementary Material 4 Table 1; SEM analysis) and consistent with reactive porous flow of initially ne-normative infiltrating melt that evolved through silica saturation (Rivalenti et al., 2004b). However, this interaction is limited to the rims of the minerals (Laurora et al., 2001; Rivalenti et al., 2004b) and therefore the cores preserve the original chemical composition.

## 6. Mineral chemistry

Previous work on the PDI xenoliths showed that primary and secondary phases are quite homogenous with negligible variations in major element composition (Ponce et al., 2015; Ponce, 2016). A similar behavior is found in our samples for both major and trace elements. For further discussion see Supplementary Material 4. We thus report and discuss averages only (olivine in Table 2; spinel in Table 3; orthopyroxene in Table 4 and clinopyroxene in Table 5) while the entire dataset of single analyses is reported as Supplementary Material 2.

### 6.1. Olivine

The forsterite (Fo, calculated as  $\text{Mg}^{2+}/(\text{Mg}^{2+}+\text{Fe}^{2+}_{\text{tot}})*100$  molar ratio) content varies between 90.6-92.3%, within the previously reported variability range of the PDI xenoliths (Rivalenti et al., 2004a). The content of NiO and CaO varies between 0.31-0.46 wt.% (61 analyses) with four analyses up to 0.86 wt.% and 0.03-0.22 wt.%, respectively (Table 2). Harzburgitic olivines commonly have higher MgO and NiO (Fig. 4-A), but lower CaO than lherzolites. Olivines from León are more relictic and have higher Fo than Matilde olivines. Chenque olivines overlap the variability fields of León and Matilde.

## 6.2. Spinel

Spinel Cr# (calculated as  $\text{Cr}^{3+}/(\text{Cr}^{3+}+\text{Al}^{3+}_{\text{tot}})*100$  molar ratio) varies between 16.6 and 77.5% and Mg# between 58.1 and 79.1% (Fig. 4-B). According to the classification of Schulze (2001), minerals are mainly spinel, but in lherzolites, harzburgites and ol-websterites from León and one harzburgite from Matilde they are magnesiochromite (Fig. 4-B). New samples from León show the highest Cr# values while the Chenque spinels have the highest Mg# (Fig. 4-B).

## 6.3. Orthopyroxene

Orthopyroxene is enstatite and its composition is in the range  $\text{En}_{86-92}$ ,  $\text{Ws}_{1-2}$  and  $\text{Fs}_{7-12}$  and Mg# (calculated as  $\text{Mg}^{2+}/(\text{Mg}^{2+}+\text{Fe}^{2+}_{\text{tot}})*100$  molar ratio) varies between 82.4 and 93.0%. The content of MgO in the majority of the orthopyroxenes ranges from 28.88 to 35.03 wt.% with Q150 websterite of Chenque with the lowest MgO content (28.88 wt.%) (Table 4). Websterites and olivine-websterites have the lowest Mg# values, between 81.4 and 87.8% with the exception of sample L90 (Fig. 4-C; Table 4). No significant distinction has been observed between orthopyroxenes of the three outcrops. Overall, our orthopyroxenes fall within the range defined by Melchiorre et al. (2020; and references therein) for North Patagonia mantle peridotites (Fig. 4-C) with the exception of the following three samples: one lherzolite from León (sample L92) and one lherzolite and one harzburgite from Chenque (samples Q155 and Q109, respectively).

## 6.4. Clinopyroxene

Clinopyroxene is diopside with  $\text{En}_{47-51}$ ,  $\text{Wo}_{44-48}$  and  $\text{Fs}_{2-7}$  composition. It is characterized by an increase of  $\text{Na}_2\text{O}$  and  $\text{Al}_2\text{O}_3$  with a decrease of CaO.  $\text{Na}_2\text{O}$  varies in the range of 0.40-1.55 wt.%,  $\text{TiO}_2$  is between 0.01-0.38 wt.%,  $\text{Cr}_2\text{O}_3$  between 0.22-1.27 wt.% and Mg# between 87.2-95.6 (Table 5). As for the orthopyroxenes, our clinopyroxenes mainly fall in

Formatted: English (United States)



the compositional field defined for North Patagonia by Melchiorre et al. (2020; and references therein) (Fig.4-D), with the exception of four clinopyroxenes from Chenque and two from León, therefore expanding the clinopyroxene compositional field reported for mantle xenoliths in this region.

## **7. Clinopyroxene trace element chemistry**

Clinopyroxene trace element composition of each sample is very homogenous and contrasts with a marked inter-sample heterogeneity. Here, we focus on the REE patterns that well picture the extreme variability in element distribution. We recognized five significant groups based on clinopyroxenes REE patterns (Fig. 5).

**Group I** clinopyroxenes are depleted in LREE and were recognized only in one lherzolite (Q155) from Chenque. This sample pattern approaches the model curves for 11-14% melting in the spinel field (Fig. 5-A). This sample is the only one approaching a near fractional melting trend.

**Group II** clinopyroxenes are characterized by patterns enriched in LREE and relatively flat to weakly concave upward. They comprise clinopyroxenes from one lherzolite (M53) and one harzburgite (M55) from Matilde, one lherzolite (L91), one harzburgite (L69) and one olivine-websterite (L90) from León, and one lherzolite (Q103) and one harzburgite (Q108) from Chenque. The LREE enrichment is clearly due to melt/rock reaction processes. However, a high degree of depletion can be inferred for a possible protolith if assuming HREEs as representative, or close to, the pre-reactive composition. These degrees of depletion require up to 20% non-modal partial melting of a primitive mantle (Fig. 5-B). Two clinopyroxene patterns from PDI xenoliths published by Rivalenti et al (2004a) have M- to H-REE that correspond to PM clinopyroxene composition (Fig. 5-B). The LREE of group II clinopyroxene are strongly fractionated, with La/Yb<sub>N</sub> between 1.3 and 68.0. Trace elements in clinopyroxenes with fractionated HREE show negative anomalies in Ba and Ti accompanied by depletion in Nb and Ta and Zr and Hf compared to “flat” samples (Fig. 5-B). Conversely, they have higher concentration for Th and U with respect to Group V. Matilde samples also show negative Pb negative anomaly.

**Group III** clinopyroxenes have V/U-shaped patterns and are found only in xenoliths from Chenque (samples Q65, Q90 and Q101) and Matilde (samples M57, M67, M79 and M82). Lherzolites show mainly V-shaped patterns with a common minimum in Nd and are the most enriched in HREE (Fig. 5-C; Sm/Yb<sub>N</sub> between 0.04 and 0.19). Harzburgites show U-shaped patterns with more fractionated and less abundant HREE (Fig. 5C; Sm/Yb<sub>N</sub> between 0.40

and 7.5). Matilde clinopyroxenes are enriched in LREE and depleted in HREE with respect to those of Chenque. They also have a higher concentration of incompatible elements such as Rb, Th, U and Ba and lower Ti compared to Chenque (Fig. 5-C). Similarly to Group II, these clinopyroxenes are enriched in Th and U and have negative anomalies in Ba, Pb and Ti.

**Group IV** clinopyroxenes have sinusoidal patterns and belong to three lherzolites (Q105, Q107, Q154) and one harzburgite (Q109) from Chenque (Fig. 5-D). They exhibit HREE patterns consistent with a primitive mantle residual clinopyroxene depleted by 8 to 20% of melt extraction. Among the clinopyroxenes showing REE patterns different from the primitive mantle (groups II-V), samples with sinusoidal REE patterns show the lowest abundances with values equal or below the primitive mantle concentration (Fig. 5-D). They show Ba negative anomaly and a variable positive to negative Pb anomaly. Ti, which in other groups shows negative anomalies, is flat or slightly depleted.

**Group V** clinopyroxenes are characterized by “flat” patterns and are represented by a number of clinopyroxenes from Chenque (samples Q58, Q77, Q80, Q150, Q152, Q153 and QEug), Matilde (sample MH) and León (samples L82 and L92) ( $La_N/Yb_N$  from 1.01 to 1.88) (Fig. 5-E). The HREE fit with a fractional melting depletion between 10 and 17%, whereas the MREE and LREE deviate from the model (Fig. 5-E). All three websterites from Chenque belong to this group. All samples show negative anomalies in Ba and slightly negative anomalies for Ti. Thorium, U, Nb and Ta vary from depleted to enriched with respect to the primitive mantle, with the lower values in websterite and the higher values in peridotites.

## 8. Geothermobarometry

We carried out geothermometrical calculations based on two pyroxene equilibria (Brey and Köhler, 1990; Taylor, 1998) and Ca-in orthopyroxene (Brey and Köhler, 1990). Temperatures were calculated for each couple with core analyses of crystals in contact with each other. Averages for each sample are reported in Table 7. An extensive discussion about the precision and accuracy of the geothermometers used is reported in Nimis and Grütter (2010). Hereafter we discuss only the estimated temperatures of Ca-in orthopyroxene geothermometer to compare our data with those of Patagonian spinel peridotites reported in the literature (e.g. Rivalenti et al., 2004a; Bjerg et al., 2005; Bertotto et al., 2013).

At Chenque, temperatures vary between  $853 \pm 15^\circ\text{C}$  (websterite Q150) and  $975 \pm 5^\circ\text{C}$  (lherzolite Q155) with an average of  $905 \pm 34^\circ\text{C}$ . Chenques' lherzolites have higher estimated T compared to the harzburgites (between  $879\text{--}975^\circ\text{C}$  and  $868\text{--}930^\circ\text{C}$ , respectively;

Table 7). In Matilde, temperatures range from 859°C (harzburgite M55) to  $1057 \pm 32^\circ\text{C}$  (harzburgite M57) with an average of  $903 \pm 76^\circ\text{C}$ . The average estimated T is higher in lherzolite ( $908 \pm 66^\circ\text{C}$ ) than in harzburgite ( $902 \pm 87^\circ\text{C}$ ) but they are comparable within errors. In León, temperatures range between  $860 \pm 44^\circ\text{C}$  (lherzolite L91) and  $981^\circ\text{C}$  (lherzolite L92) with an average T of  $914 \pm 45^\circ\text{C}$ . Similarly to Chenque and Matilde, lherzolite in León shows higher average T with respect to harzburgite ( $920 \pm 86^\circ\text{C}$  and  $899 \pm 10^\circ\text{C}$ , respectively).

The equilibrium pressures were estimated based on the Mercier (1980) clinopyroxene geobarometer and *vary varied* between  $1.4 \pm 0.3$  and  $2.9 \pm 0.1$  GPa in Chenque, between 1.4 and  $3.7 \pm 1.3$  GPa in Matilde and between 1.6 and  $2.7 \pm 0.1$  GPa in León (Table 7 and Fig. 6). We note here that in *the* literature (see discussion in Yang et al., 1998), it is well known that pressure estimations in the spinel field could be affected by large errors (e.g.  $3.7 \pm 1.3$  GPa) and that the best estimates are given by Mercier (1980) geobarometer.

The comparison of the entire PDI data set (Ponce et al., 2015; and this work) with estimated temperatures for Patagonian spinel peridotites reported in literature shows that the lowest temperatures are indeed those of the PDI samples (Fig. 6). Bjerg et al. (2005) previously reported a T of  $1030^\circ\text{C}$  for a PDI harzburgite (CH16-A), and Rivalenti et al. (2004a) estimated a T interval between 839 and  $1197^\circ\text{C}$  for eight mantle xenoliths in this area. The overall range of temperatures of the studied xenoliths varies between  $853 \pm 15$  and  $1057 \pm 32^\circ\text{C}$ , with an average of  $906 \pm 47^\circ\text{C}$ .

## 9. Discussion

### 9.1. Mantle source and melting processes

As shown by the mineral modal composition, the studied peridotites are markedly depleted. The abundance of harzburgites and lherzolites with less than 6% clinopyroxene suggests that the mantle column below the PDI area is significantly more depleted than the primitive mantle reference (Warren, 2016; Fig. 2). This is true for most of the Patagonian mantle xenoliths described in literature (Laurora et al., 2001; Rivalenti et al., 2004a, 2007a, 2007b; Bjerg et al., 2005) suggesting that the regional mantle is strongly depleted. However, the age of this depletion process is still controversial. According to Schilling et al. (2008), xenoliths from the North Patagonian Massif (comprising those of the PDI area) have a range in  $^{187}\text{Os}/^{188}\text{Os}$  similar to modern oceanic peridotites with  $T_{\text{RD}}$  and  $T_{\text{MA}}$  ages varying from 0.03 to 0.98 Ga, indicative of a relatively recent lithospheric mantle formation process from a convecting mantle. Granulite xenoliths from the PDI area have been dated by U-Pb SHRIMP

zircon ages to  $175.9 \pm 4.9$  Ma (Castro et al., 2011), which is interpreted as the formation time of this residual lithosphere.

The refractory character of the mineral associations is consistent with the bulk composition, with MgO abundances similar to the more depleted spinel facies xenoliths of Patagonia (Supplementary Material 1 Table 1). Accordingly, the major elements composition of mineral phases is mainly Al-poor and Mg and Cr-rich (Tables 2 to 5).

The chemical composition of mineral phases and the variation in modal composition of the PDI xenoliths do not follow a melting trend. In comparison with the modal and mineral composition of global abyssal residual mantle (Warren et al., 2016), a reference for near fractional (extraction-dominated) melting processes in the mantle, and in particular with peridotites from the Vema Lithospheric Section, representative of the integrated melting events over a single mantle parcel (Brunelli et al., 2006; Cipriani et al., 2009), the PDI mantle rocks show an excess of clinopyroxene, Yb and higher Cr# for both clinopyroxene and spinel (Fig. 7). PDI pyroxenes appear to be more residual than abyssal peridotites, having higher Mg# and lower  $Al_2O_3$  (Fig. 7), but unexpectedly, they have lower  $Cr_2O_3$  than abyssal rocks (Fig. 7). Cr behaving as compatible during melting is expected to be higher for these Al and Mg values. At the same time, clinopyroxene  $Na_2O$  is higher than in the abyssal rocks.

These relationships are consistent with extensive melt-rock reactions resulting in a decoupling between modal and chemical compositions of the xenoliths (Fig. 7). High Na contents and positive Na-Cr correlations in clinopyroxene are indicative of reactions with Na-rich/Cr-poor melts under near-batch conditions as shown by Seyler and Brunelli (2018).

The lack of correlation between modal composition and mineral chemistry is shown by both major and trace elements (see Table 1; Fig. 7). For instance, no correlation between mode and chemical indicators of the degree of depletion is observed when grouping samples by clinopyroxene abundance (Fig. 7A, B). The observed modal-chemical distribution falls outside of the residual mantle array used to calibrate melting proxies such as Cr# or  $Yb_N$  (e.g. Warren, 2016), therefore a relative degree of melting cannot be inferred for our sample suite. Overall the PDI xenoliths indicate a remarkable depletion of the mantle column prior to the younger metasomatic/refertilization processes generating the observed REE patterns and the modal distribution.

Moreover, the variation of modal composition of the PDI xenoliths cannot be reproduced by the simple melting of a PM or DM mantle (Fig. 2B). With the exclusion of the websteritic samples, the two pyroxenes are related to olivine by complex trends, with a general

decreasing of orthopyroxene by increasing olivine and the persistence of clinopyroxene even at very high olivine contents (Fig. 2B).

At low olivine contents, orthopyroxene exceeds the expected composition for the modal variation of a residual mantle after melt extraction in the spinel facies. This suggests the presence of inherited local orthopyroxene-rich and clinopyroxene-poor regions in the PDI mantle before the last refertilization process. High modal orthopyroxene can result from fluid-assisted partial melting by injection of Si-rich melts as those originated in a subducted slab (e.g. Mazzucchelli et al., 2009; Zanetti et al., 2016; Jing et al., 2019; Giovanardi et al., 2020).

The general modal decrease in orthopyroxene and clinopyroxene at increasing olivine follows the “normal” depletion trend in the spinel field:  $\text{opx}+\text{cpx}+\text{melt1} \rightarrow \text{ol}+\text{melt2}$ .

However, steep trends of decreasing orthopyroxene and increasing clinopyroxene suggest that the last melting event was marked by melt/rock interaction in which clinopyroxene crystallized at the expense of orthopyroxene. The instability of orthopyroxenes is confirmed by the petrographic observations of secondary olivine replacing large orthopyroxene in olivine rich peridotites (Fig. 3E, H). This evidence suggest that the main melt/rock reaction during the melting process follows the reaction:  $\text{opx}+\text{melt1} \rightarrow \text{ol}+\text{melt2}\pm\text{cpx}$ .

Experimental studies have shown that under hydrous conditions the orthopyroxene stability field is reduced by the expansion of olivine and clinopyroxene fields in the spinel-facies (e.g. see Fig. 3 in Asimow and Longhi, 2004). We stress therefore that the decreasing opx/cpx modal trends have been possibly generated under hydrous conditions.

The low clinopyroxene Cr content can be explained by the formation of pyroxenes by reaction with Cr-poor melts (as all mantle-derived melts are) and thus sustaining further the process of clinopyroxene crystallization during melt/rock reaction. This reasoning is however complicated by the fact that also orthopyroxene is depleted in Cr and Al (Table 4).

If only clinopyroxene is generated during melting, assuming a short equilibration time, we should expect the orthopyroxene to record a more “residual” fingerprint (i.e. higher Cr for a given Al content). However, the two pyroxenes are clearly equilibrated to low Cr, thus suggesting an efficient re-equilibration during melt/rock reaction hiding the different genesis of the two minerals. The low Cr content can also be a clue to the origin of the orthopyroxene enrichment. It would point to a reactive origin in the presence of melt, such as an open-system melting in a hydrous environment deep in the garnet stability field. This suggests that melting before the last event largely occurred in the garnet-facies followed by decompression in the spinel stability field where the orthopyroxene consuming reaction

occurred. This scenario is compatible with a mantle parcel rising within a suprasubduction setting being percolated by hydrous melts derived from deep slab dehydration. A first extreme depletion episode with large orthopyroxene crystallization in the garnet facies is followed by a shallower (spinel-facies) event where orthopyroxene is frequently consumed in favor of clinopyroxene. The low Al, Fe and high Mg contents described are therefore related to depletion processes associated with long integrated melt extraction. The exception shown by Cr might be a proof of the progressive clinopyroxene crystallization and at the same time a consequence of the orthopyroxene enrichment in the source before the last melt/rock reaction event.

Overall the melting process hints at the last melt/rock reaction and melt extraction events occurring in open-system conditions. This is also suggested by the clinopyroxene trace element composition. Mildly incompatible trace elements are overall depleted; the patterns variability and the partial enrichment of the most incompatible elements may mask the overall paucity of the incompatible content (Fig. 5). During melt/rock reaction the HREE are barely modified and usually hard to be enriched under different P-T conditions and chemical composition of the infiltrating melt (Ozawa, 2001; Brunelli et al., 2014). The overall depletion of the PDI pyroxenes rules out the possibility of pure melt trapping as the leading process. A large pattern and enrichment variability can instead be created during conditions of open-system melting with melt infiltration (see model patterns in Brunelli et al., 2014). In an open-system scenario the HREE is generally depleted by progressive melt extraction with negligible effect on their abundances by the infiltrating melt.

The compositional variability observed also suggests a variation of the apparent degree of melting that cannot be justified in terms of lateral variations of temperature due to the small distance between the eruptive centers. Moreover, the modal and chemical variabilities are extremely high within the same locality (Fig.s 2 and 5). Lack of any correlation between modal and chemical composition may suggest that we are observing the results of a process acting at a small scale, for both geometry (size of reacting cells) and composition (variability of the percolating melts with respect to the composition of the percolated cell).

It means that percolating processes act over a short-scale (meter), thus making impossible to disentangle single events. Partial melting may be locally enhanced by progressive melt channeling which includes dissolution of pyroxenes, compositionally mimicking the melt-depletion tendency (Kelemen, 1990). In this context, the occurrence of dunites in the PDI area (Rivalenti et al., 2004a; Bjerg et al., 2005) can be interpreted as representing extreme

terms of pyroxene dissolution due to the channeling of silica sub-saturated melts to relatively low pressure (Mazzucchelli et al., 2009).

#### 9.2. Melt/rock reactions

As previously discussed, evidence shows that the xenolith endured at least two reactive events during the last melting process along with the infiltration of the host-basalt at low pressure (Fig. 3; Supplementary Material 4). The infiltration of the host basalt occurred through decompressional fractures originated during the dismembering of the mantle and the extraction of the xenoliths during mechanical relaxation. In such conditions, the carrying melt modified only the chemical composition of the xenoliths' minerals at the rim, in contact with the host basalt or with intruding veins (Laurora et al., 2001; Rivalenti et al., 2004b; Fig. 3G; Supplementary Material 4).

The last main melting process within the PDI mantle column produced instead an homogenization of the mineral composition as observed by the similar composition of primary and secondary minerals within the same sample (Supplementary Material 4). The fluids/melts modified the trace element imprint as observed in the variable REE and extended patterns of clinopyroxene, mostly incongruent with the fractional melting model (Fig. 5). As previously discussed, it is difficult to disentangle the melt/rock reactions and the melting process.

Group I sample seems the least affected by melt/rock reactions as seen in the REE pattern and modal composition. A similar pattern was recognized in clinopyroxenes from group 1 of Agua Poca (Bertotto et al., 2013), which also show comparable Th and U concentrations. The clinopyroxene trace elements concentration, with almost flat HREE and MREE, is consistent with non-modal fractional melting in spinel-facies conditions (Fig. 5). Modeling of the melt in equilibrium with the clinopyroxene of Group I (Fig. 8-A; clinopyroxene/melt partition coefficient are from Ionov et al., 2002) is consistent with a depleted melt.

Group V 'flat' patterns are characterized by uniform values of L- and MREE and are enriched compared to the non-modal fractional melting modeled clinopyroxene composition. This behavior suggests a more prolonged melt/rock interaction episode compared to Group II, III and IV xenoliths, with the residual mantle of this region attaining relative equilibrium with the interacting melt. Similar parallel, almost horizontal patterns have been observed in clinopyroxenes from Cerro de los Chenques (160 km SW of PDI; Rivalenti et al., 2007a) and from Cerro Chenque (north of the Somuncurá plateau, Mundl et al., 2015). Potential melts in equilibrium with the clinopyroxene of Group V are the best candidates for the

original composition of this migrating melt because of the longer melt/rock interaction with respect to the other clinopyroxenes. The melt in equilibrium with Group V is calculated using the clinopyroxene/melt partition coefficients of Green et al. (2000) and Hauri et al. (1994). The resulting composition is similar to Patagonian arc basalts or adakitic-like melt (Fig. 8-B).

We modeled melt-rock reactions in the PDI mantle column using the approach proposed by Brunelli et al. (2014) based on the equation system of Ozawa and Shimizu (1995) and Ozawa (2001). In particular we will address the general variations in modal composition and REE patterns of Group II, III and IV. Used parameters are  $F$ = degree of melting,  $\beta$ = influx melt rate,  $f_p$ = critical mass porosity and  $\phi$ = actual porosity.  $\phi/F$  is the porosity/melting ratio and is used as proxy for the type of melting process: a pure batch melting has  $\phi/F = 1$  (where all the produced melt is retained in the system) while pure fractional melting has  $\phi/F = 0$  (where the system porosity does not permit the retention of the melt). Mineral melting coefficients ( $X$ ) determine their dissolution (positive) or crystallization (negative). Details and equations are in Brunelli et al. (2014).

The mantle original modal composition was estimated as: olivine 58.3%, orthopyroxene 35.0%, clinopyroxene 4.7% and spinel 2.0%. Modes for dry melting are from Brunelli et al. (2006), for hydrous melting are from Grove and Till (2019) (garnet-facies) and from Bizimis et al. (2000) (spinel-facies). The processes were modeled using melt compositions of Patagonian adakites (Stern and Kilian, 1996) similar to melts in equilibrium with Group V clinopyroxene. Modelling the process previously described requires the creation of a large clinopyroxene excess by reaction and contextual melt extraction. Melt extraction is required by the progressive depletion of HREE and Al and the increase of Mg. Orthopyroxene consumption appears to have a random correlation with clinopyroxene modal content. This suggests a significant variation of the reaction coefficients of the process at different moments.

The stochastic distribution of the different pattern shapes with respect to the modal distribution suggests that these rocks experienced a short scale melt/rock reaction, overprinting an extremely variable protolith and with extremely variable melt composition. Therefore, a general model cannot be extrapolated. Only part of the process can be modeled congruently. Here, we focus on some significant examples showing how different patterns can possibly be generated setting some constraints on the composition of the melt and the intensive process parameters ( $\phi$ - $F$ - $\beta$ -reaction mode). A general character that can be assumed is the depleted nature of the protolith in term of incompatible elements. We hence



assume a depleted starting clinopyroxene in the calculations (similar to Group I) and low modal clinopyroxene in the starting assemblage, assuming that the majority of this mineral is created by reaction as already discussed. For this reason, melting coefficients are always high for orthopyroxene and low or negative for clinopyroxene. Chromatographic effects must also be considered as shown by V-shaped REE patterns in Group III (Fig. 5). We thus create models in spinel-facies conditions considering the chromatographic effects and pure incremental open system (Fig. 9). The latter represents the end member case in which the inflowing melt always has the same composition, thus a case representative of a process in which melt is supplied by an external reservoir (as for instance a melt channel) that adds fresh melt of constant composition at each step. In this configuration chromatographic effects are therefore not visible.

The main melting trend, i.e. depletion in pyroxenes and crystallization of olivine, requires positive coefficients for orthopyroxene and clinopyroxene. Positive coefficients mean consumption of both phases during the reaction. This model follows the upper limit of the maximum pyroxenes trend with respect to olivine thus considering high orthopyroxene content in the source (Fig. 9A). The most favorable case is given by  $X_{Opx} = 0.7$  and  $X_{Cpx} = 0.1$ . For this case,  $\phi/F$  and  $\beta$  can only have intermediate values, both set at 0.40 and using the adakite as influxing melt. Modal variations are consistent with the main pyroxenes depletion trends (Fig. 9A). Resulting REE patterns for chromatographic effects show extreme enrichments in LREE (Fig. 9A). The chromatographic model matches the REE patterns of the most enriched samples of Group II and III (Fig. 9A).

To simulate the modal trend enriching the system in clinopyroxene at the expense of orthopyroxene, which crosscut the main trend at high orthopyroxene content, we need to set the  $X_{Cpx}$  as negative. Patterns become significant at  $\beta > 0.2$  and a low  $\phi/F = 0.3$  (thus increasing the fractional melting): the resulting pattern considering the chromatographic effect shows a sinusoidal shape (Fig. 9B). Under this configuration, increasing the  $\phi/F$  value (thus increasing the batch process) results in relatively more enriched patterns with a shape changing progressively to concave while the modal variation remains constant (Fig. 9C). These patterns could match the Group IV for high fractional melting ( $\phi/F = 0.2$ ; Fig. 9B) and Group III for a higher batch process ( $\phi/F = 0.6$ ; Fig. 9C). Similar sinusoidal patterns as Group IV have been recognized in two xenoliths from Prahuaníyeu: Pra1 of Mundl et al. (2015) and Pra68 from Group 3 of Bjerg et al. (2009). Concave LREE-enriched patterns were instead recognized in clinopyroxenes from Prahuaníyeu, Pra304 from Group 1 of Bjerg et al. (2009), and Pr301 and 303 from north of the Somuncurá plateau (Mundl et al., 2015).

If we consider the pure incremental open system with the same conditions and high batch process (i.e.  $\phi/F=0.6$ ), the resulting pattern shows almost flat HREE (Fig. 9C). This pattern is similar to most of Group II samples. Similar patterns in Patagonia were recorded, among others, in clinopyroxenes from Puesto Díaz (north of the Somuncurá plateau; Mundl et al., 2015) and in clinopyroxenes from Group 2 of Bjerg et al. (2009) from Prahuaníyeu (Somuncurá plateau). Rivalenti et al. (2007a) proposed a numerical simulation of a chromatographic enrichment for similar patterns in Cerro de los Chenques xenoliths (160 km SW of PDI).

The pattern relationships observed before remain valid at low orthopyroxene content: changes in the melting coefficients produce the same changes in the pattern morphology (Fig. 9D-G). This is true for the vertical pyroxene trend (Fig. 9D), the pyroxene dispersion toward (extremely) low orthopyroxene contents with some residual clinopyroxene (Fig. 9E) or the extreme case that considers depletion of both pyroxenes (Fig. 9F-G).

### 9.3 Regional events

A regional model for the metasomatic/refertilization events of northern Patagonia reported the occurrence of two distinct melt percolations in the mantle column (Melchiorre et al. 2020). According this model, the first metasomatic event occurred after partial melting of the mantle column by percolation of a tholeiitic depleted basalt, which depleted the clinopyroxene in LREE. The second event was induced by percolation of alkaline to transitional SiO<sub>2</sub>-undersaturated melts, which produced limited refertilization with LREE enrichment in clinopyroxene. These two events have been related to the Patagonian plateau magmatism where large volumes of tholeiitic lavas are followed by limited pulses of alkaline melts (Gorring et al., 2003; D'Orazio et al., 2004; Kay et al., 2007, 2013; Melchiorre et al., 2020). These events, however, are not identical in all the northern Patagonian regions but change locally (Melchiorre et al., 2020; and references therein). This is the case of the PDI area.

As previously discussed, the last melting event in the studied area and their associated melt/rock reactions overprinted the previous mantle composition. In particular, several different REE patterns and modal compositions could be obtained from the same melting event when melt influx rate and porosity change. This is taken to the extreme if the mantle column was, as certainly was, already heterogeneous by previous processes. Modal and chemical variations of mantle xenoliths of PDI could be obtained from an open-system melting process due to the influx of an adakitic melt. In addition, the LREE-depleted samples

(Group I), previously interpreted as related to a tholeiitic metasomatism (Melchiorre et al., 2020), could be explained by fractional melting in spinel conditions. These evidences indicate that the PDI mantle column has been completely overprinted by the alkaline/adakitic melting event (Fig. 10). The tholeiitic event, if occurred, is now completely overprinted. Similar geochemical features from several other Patagonian xenoliths (e.g. Puesto Díaz, Prahuaní, Cerro de los Chenques, Cerro Chenque; Rivalenti et al., 2007a; Bjerg et al., 2009; Mundl et al., 2015) suggest that open-system melting could be responsible for mantle heterogeneity in the Patagonian region.

## 10. Conclusions

The abundance of harzburgites and lherzolites with less than 6% clinopyroxene by volume (~70% of all samples) confirms that the mantle column below the Paso de Indios area is significantly depleted with respect to the modal composition of the primitive mantle. Petrological evidence of garnet breakup suggests that melting started in garnet-facies and continued in spinel facies driven by the influx of an adakitic melt. This melt is related to the subduction process active along the western margin of South America since Late Triassic times.

The melting process was open-system, inducing melt/rock reactions that produced modal and compositional heterogeneities on a small scale. These processes completely overprinted the original mantle composition and previous processes. Heterogeneities were produced by different degrees of melt influx and rock porosity, which are the main factors controlling the nature of the melting process from complete fractional to mainly batch (up to 60%).

Among the several Patagonian localities with outcropping subcontinental mantle xenoliths, the PDI xenoliths are unique. Here, the mantle can be studied in different stages, from the initial pre-subduction depletion to the late superimposed melt/rock reaction events during open-system melting.

## Acknowledgements

We thank the Facultad de Ciencias Exactas y Naturales (Universidad Nacional de La Pampa, Argentina), CNR–CONICET joint program and Programmi di Ricerca di Interesse Nazionale of the Italian Ministero dell'Istruzione, dell'Università e della Ricerca (protocol PRIN 20178LPCPW) project for financial support. DB is supported by PRIN 2017KY5ZX8 funding. We thank Guest Editor Prof. Zaffarana and two anonymous reviewers for constructive comments which helped to improve this work.

644

## 645 References

- 646 Acevedo, R.D., Quartino, B.J., 2004. Basalto alcalino portador de xenolitos ultramáficos en  
647 Tierra del Fuego. *Revista de la Asociación Geológica Argentina* 59, 411-415.
- 648 Alric, V., Labudía C., Iglesias C., Pardo M., 1993. Xenolitos lherzolíticos en basaltos  
649 alcalinos del centro de la provincia del Chubut. Decimosegundo Congreso Geológico  
650 Argentino y segundo Congreso de Exploración de Hidrocarburos, Mendoza, Argentina.  
651 *Actas* 4, 249-255.
- 652 Alric, V., 1996. Los basaltos portadores de xenolitos aflorantes en las localidades Paso de  
653 Indios y Cerro Cándor, departamento de Paso de Indios, provincia del Chubut (Ph.D.  
654 Thesis). Universidad Nacional de la Patagonia San Juan Bosco, Argentina.
- 655 Alric, V., Haller, M., Féraud, G., Bertrand, H., 2002. Volcanismo Alcalino Paleógeno en los  
656 alrededores de Paso de Indios, provincia del Chubut. Decimoquinto Congreso Geológico  
657 Argentino, El Calafate, Argentina. *Actas* 2, 101-106.
- 658 Anders, E., Grevesse, N., 1989. Abundances of the elements: meteoritic and solar.  
659 *Geochimica et Cosmochimica Acta*, 53, 197-214. [10.1016/0016-7037\(89\)90286-X](https://doi.org/10.1016/0016-7037(89)90286-X)
- 660 Anselmi, G., Gamba, M., Panza, J., 2004. Descripción geológica de la Hoja 4369-IV, Los  
661 Altares, Provincia del Chubut. Servicio Geológico Minero Argentino. Boletín N° 313,  
662 Buenos Aires, Argentina.
- 663 Aragón, E., D'Eramo, F., Castro, A., Pinotti, L., Brunelli, D., Rabbia, O., Rivalenti, G.,  
664 Varela, R., Spakman, W., Demartis, M., Cavarozzi, C., Aguilera, Y., Mazzucchelli, M.,  
665 Ribot, A., 2011. Tectono-magmatic response to major convergence changes in the north  
666 Patagonian suprasubduction system: The Paleogene subduction-transcurrent plate margin  
667 transition. *Tectonophysics*, 509, 218-237. <https://doi.org/10.1016/j.tecto.2011.06.012>
- 668 Aragón, E., D'Eramo, F., Pinotti, L., Aguilera, Y., Cavarozzi, C., Demartis, M., Gomez  
669 Dacal, L., Castro, A., Rabbia, O., Hernando, I., Fuentes, T., 2015. El rift invertido  
670 Paleógeno de los Patagonides, Patagonia septentrional: evolución y cambios de estilo  
671 extensional. Decimocuarto Congreso Geológico Chileno, Valparaíso. *Actas* 1, 162-165.
- 672 Arai, S., 1994. Characterization of spinel peridotites by olivine-spinel compositional  
673 relationships: review and interpretation. *Chemical Geology*, 113, 191-204.  
674 [https://doi.org/10.1016/0009-2541\(94\)90066-3](https://doi.org/10.1016/0009-2541(94)90066-3)
- 675 Ardolino, A., Franchi, M., 1993. El vulcanismo cenozoico de la meseta de Somún Cura,  
676 provincias de Río Negro y Chubut. Decimosegundo Congreso Geológico Argentino,  
677 Buenos Aires, Argentina. *Actas* 4, 225-235.
- 678 Asimow, P. D., & Longhi, J. (2004). The significance of multiple saturation points in the  
679 context of polybaric near-fractional melting. *Journal of Petrology*, 45(12), 2349-  
680 2367.
- 681 Barbieri, M.A., Rivalenti, G., Cingolani, C., Vanucci, R., Kempton P., 1999.  
682 Geochemical and isotope constraints on the composition of the mantle lithosphere in  
683 Patagonia (Argentina, Chile). Second South American Symposium on Isotope Geology,  
684 Carlos Paz, Argentina. *Actas* 2, 163-166.
- 685 Bertotto, G.W., 2000. Cerro Agua Poca, un cono basáltico cuaternario portador de xenolitos  
686 ultramáficos, en el oeste de la provincia de La Pampa, Argentina. *Revista de la Asociación  
Geológica Argentina*, 55, 59-71.
- 687 Bertotto, G.W., Mazzucchelli, M., Zanetti, A., Vannucci, R., 2013. Petrology and  
688 geochemistry of the back-arc lithospheric mantle beneath eastern Payunia (La Pampa,  
689 Argentina): Evidence from Agua Poca peridotite xenoliths, *Geochemical Journal*, 47,  
690 219-234. <https://www.terrapub.co.jp/journals/GJ/pdf/4702/47020219.pdf>

Formatted: English (United States)

Formatted: English (United States)

Formatted: English (United States)

- 691 Bizimis, M., Salters, V. J., & Bonatti, E. (2000). Trace and REE content of clinopyroxenes  
692 from supra-subduction zone peridotites. Implications for melting and enrichment  
693 processes in island arcs. *Chemical Geology*, 165(1-2), 67-85.
- 694 Brunelli, D., Seyler, M., Cipriani, A., Ottolini, L., & Bonatti, E. (2006). Discontinuous melt  
695 extraction and weak refertilization of mantle peridotites at the Vema lithospheric section  
696 (Mid-Atlantic Ridge). *Journal of Petrology*, 47(4), 745-771.
- 697 Brunelli, D., Paganelli, E., & Seyler, M. (2014). Percolation of enriched melts during  
698 incremental open-system melting in the spinel field: A REE approach to abyssal  
699 peridotites from the Southwest Indian Ridge. *Geochimica et Cosmochimica Acta*, 127,  
700 190-203.
- 701 Bjerg, E.A., Labudía, C., Cesaretti, N., 1991. Mineralogy, texture and stress measurements  
702 of mantle xenoliths from Southern Argentina. *Berichte der Deutschen Mineralogischen*  
703 *Gesellschaft. Beihefte zum: European Journal of Mineralogy*, 3, 31.
- 704 Bjerg, E.A., Ntaflos, Th., Kurat, G., Dobosi, G., Labudia, C., 2005. The upper mantle  
705 beneath Patagonia, Argentina, documented by xenoliths from alkali basalts. *Journal of*  
706 *South American Earth Sciences*, 18, 125-145.  
707 <https://doi.org/10.1016/j.jsames.2004.09.002>
- 708 Bjerg, E.A., Ntaflos, Th., Thöni, M., Aliani, P., Labudia, C., 2009. Heterogeneous  
709 lithospheric mantle beneath Northern Patagonia: evidence from Prahuaníyeu garnet- and  
710 spinel-peridotites. *Journal of Petrology*, 50, 1267-1298.  
711 <https://doi.org/10.1093/petrology/egp021>
- 712 Brey, G., Köhler, T., 1990. Geothermobarometry in four-phase lherzolites II. New  
713 thermobarometers, and practical assessment of existing thermobarometers. *Journal of*  
714 *Petrology* 31, 1353-1378. <https://doi.org/10.1093/petrology/31.6.1353>
- 715 Castro, A., Aragón, E., Díaz-Alvarado, J., Blanco, I., García-Casco, A., Vogt, K., Liu, D.,  
716 2011. Age and composition of granulite xenoliths from Paso de Indios, Chubut province,  
717 Argentina. *Journal of South American Earth Sciences*, 32, 567-574.  
718 <https://doi.org/10.1016/j.jsames.2011.06.001>
- 719 Cipriani, A., Bonatti, E., Brunelli, D., & Ligi, M. (2009). 26 million years of mantle  
720 upwelling below a segment of the Mid Atlantic Ridge: The Vema Lithospheric Section  
721 revisited. *Earth and Planetary Science Letters*, 285(1-2), 87-95.
- 722 Correia, C.T., Sinigoi, S., Girardi, V.A.V., Mazzucchelli, M., Tassinari, C.C.G., Giovanardi,  
723 T., 2012. The growth of largemafic intrusions: comparing Niquelandia and Ivrea igneous  
724 complexes. *Lithos*, 155, 167–182. <http://dx.doi.org/10.1016/j.lithos.2012.08.024>
- 725 Cotten, J., Le Dez, A., Bau, M., Caroff, M., Maury, R.C., Dulski, P., Fourcade, S., Bohn,  
726 M., Brousse, R., 1995. Origin of anomalous rare-earth element and yttrium enrichments  
727 in subaerially exposed basalts: evidence from French Polynesia. *Chemical Geology* 119,  
728 115-138. [https://doi.org/10.1016/0009-2541\(94\)00102-E](https://doi.org/10.1016/0009-2541(94)00102-E)
- 729 D'Orazio, M., Innocenti, F., Manetti, P., Tamponi, M., Tonarini, S., González-Ferràn, O.,  
730 Lahsen, A., Omarini, R., 2003. The Quaternary calc-alkaline volcanism of the Patagonian  
731 Andes close to the Chile triple junction: geochemistry and petrogenesis of volcanic rocks  
732 from the Cay and Maca volcanoes (~45°S, Chile). *Journal of South American Earth*  
733 *Sciences*, 16, 219-242. [https://doi.org/10.1016/S0895-9811\(03\)00063-4](https://doi.org/10.1016/S0895-9811(03)00063-4)
- 734 D'Orazio, M., Innocenti, F., Manetti, P., Haller, M.J., 2004. The Cenozoic back-arc  
735 magmatism of the southern extra-Andean Patagonia (44.5-52° S): a review of  
736 geochemical data and geodynamic interpretations. *Rev. Asoc. Geol. Argentina* 59 (4),  
737 525–538.
- 738 Douglas, B., Saul, S., Stern, C., 1987. Rheology of the upper mantle beneath southernmost  
739 South America inferred from peridotite xenoliths. *Journal of Geology*, 95, 241-253.  
740 <https://doi.org/10.1086/629122>

Formatted: English (United States)

Formatted: English (United States)

Formatted: English (United States)

Formatted: English (United States)

741 Echaurren, A., Folguera, A., Gianni, G., Orts, D., Tassara, A., Encinas, A., Giménez, M.,  
 742 Valencia, V., 2016. Tectonic evolution of the North Patagonian Andes (41°–44° S)  
 743 through recognition of syntectonic strata. *Tectonophysics* 677, 99–114.  
 744 Echaurren, A., Gianni, G.M., Paz, L.F., Navarrete, C., Oliveiros, V., Encinas, A., Giménez,  
 745 M., Lince-Kingler, F., Folguera, A., 2019. Tectonic controls on the building of the North  
 746 Patagonian fold-thrust belt (~43°S). *Andean Tectonics*, 609–650  
 747 Faccini, B., Bonadiman, C., Coltorti, M., Grégoire, M., Siena, F., 2013. Oceanic material  
 748 recycled within the sub-patagonian lithospheric mantle (Cerro del Fraile, Argentina).  
 749 *Journal of Petrology* 54, 1211–1258. <https://doi.org/10.1093/petrology/egt010>  
 750 Fernández Paz, L., Litvak, V.D., Echaurren, A., Iannelli, S.B., Encinas, A., Folguera, A.,  
 751 Valencia, V., 2018. Late Eocene volcanism in North Patagonia (42°30'–43°S): arc  
 752 resumption after a stage of within-plate magmatism. *J. Geodyn.*, 113, 13–31.  
 753 <https://doi.org/10.1016/j.jog.2017.11.005>.  
 754 Gelós, E., Hayase, K., 1979. Estudio de las inclusiones peridotíticas en un basalto de la  
 755 región de Comallo y de otras localidades de las provincias de Río Negro y Chubut.  
 756 *Proceedings of the 6° Congreso Geológico Argentino, Bahía Blanca (Buenos Aires),*  
 757 *Argentina. Asociación Geológica Argentina, Buenos Aires.* 2: 69–82.  
 758 Giacosa, A., Márquez, M., 1999. Jurásico y Cretácico de la Cordillera Patagónica  
 759 septentrional y Precordillera patagónica. *Instituto de Geología y Recursos minerales.*  
 760 *Geología Argentina. Anales* 29 (6): 444–459.  
 761 Giovanardi, T., Mazzucchelli, M., Lugli, F., Girardi, V.A.V., Correia, C.T., Tassinari,  
 762 C.C.G., Cipriani, A., 2018. Isotopic constraints on contamination processes in the tonian  
 763 Goiás stratiform complex. *Lithos*, 310–311, 136–152.  
 764 <https://doi.org/10.1016/j.lithos.2018.04.008>  
 765 Giovanardi, T., Girardi, V.A.V., Teixeira, W., Mazzucchelli, M., 2019. Mafic dyke swarms  
 766 at 1882, 535 and 200 Ma in the Carajás region, Amazonian Craton: Sr–Nd isotopy, trace  
 767 element geochemistry and inferences on their origin and geological settings. *Journal of*  
 768 *South American Earth Sciences*, 92, 197–208.  
 769 <https://doi.org/10.1016/j.jsames.2019.02.017>  
 770 Giovanardi, T., Zanetti, A., Dallai, L., Morishita, T., Hémond, C., Mazzucchelli, M., 2020.  
 771 Evidence of subduction-related components in sapphirine-bearing gabbroic dykes (Finero  
 772 phlogopite–peridotite): Insights into the source of the Triassic–Jurassic magmatism at the  
 773 Europe–Africa boundary. *Lithos*, 356–357, <https://doi.org/10.1016/j.lithos.2020.105366>.  
 774 Gorrington, M.L., Singer, B., Gowers, J., Kay, S.M., 2003. Plio-Pleistocene basalts from the  
 775 Meseta del Lago Buenos Aires, Argentina: Evidence for asthenosphere–lithosphere  
 776 interactions during slab window magmatism. *Chem. Geol.* 193, 215–235.  
 777 Green, T.H., Blundy, J.D., Adam, J., Yaxley, G.M., 2000. SIMS determination of trace  
 778 element partition coefficients between garnet, clinopyroxene and hydrous basaltic liquids  
 779 at 2–7.5 GPa and 1080–1200 °C. *Lithos*, 53, 165–187. [10.1016/S0024-4937\(00\)00023-2](https://doi.org/10.1016/S0024-4937(00)00023-2)  
 780 Grove, T.L., Till, C.B., 2019. H<sub>2</sub>O-rich mantle melting near the slab–wedge interface.  
 781 *Contributions to Mineralogy and Petrology*, 174, 80. [https://doi.org/10.1007/s00410-019-](https://doi.org/10.1007/s00410-019-1615-1)  
 782 [1615-1](https://doi.org/10.1007/s00410-019-1615-1).  
 783 Harte, B., 1977. Rock nomenclature with particular relation to deformation and  
 784 recrystallization textures in olivine bearing xenoliths. *The Journal of Geology*, 85(3), 279–  
 785 288. [www.jstor.org/stable/30066247](http://www.jstor.org/stable/30066247)  
 786 Hauri, E.H., Wagner, T.P., Grove, T.L., 1994. Experimental and natural partitioning of Th,  
 787 U, Pb and other trace elements between garnet, clinopyroxene and basaltic melts.  
 788 *Chemical Geology*, 117, 149–166. [https://doi.org/10.1016/0009-2541\(94\)90126-0](https://doi.org/10.1016/0009-2541(94)90126-0)  
 789 Hickey, R.L., Frey, F.A., Gerlach, D.C., López-Escobar, L., 1986. Multiple sources for  
 790 basaltic arc rocks from the southern volcanic zone of the Andes (34°–41°S): trace element

Formatted: English (United States)

Formatted: English (United States)

Formatted: English (United States)

Formatted: English (United States)

and isotopic evidence for contributions from subducted oceanic crust, mantle, and continental crust. *Journal of Geophysical Research*, 91, 5963-5983. <https://doi.org/10.1029/JB091iB06p05963>

Iannelli, S.B., Litvak, V.D., Fernández Paz, L., Folguera, A., Ramos, M.E., Ramos, V.A., 2017. Evolution of Eocene to Oligocene arc-related volcanism in the North Patagonian Andes (39–41°S), prior to the break-up of the Farallon plate. *Tectonophysics*, 696–697, 70–87. <https://doi.org/10.1016/j.tecto.2016.12.024>.

Ionov, D.A., Bodinier, J.L., Mukasa, S.B., Zanetti, A., 2002. Mechanisms and sources of mantle metasomatism: major and trace element compositions of peridotite xenoliths from Spitsbergen in the context of numerical modelling. *Journal of Petrology*, 43, 1–41.

Jalowitzki, T.L.R., Conceição, R.V., Orihashi, Y., Bertotto, G.W., Nakai, S., Schilling, M., 2010. Evolução geoquímica de Peridotitos e Piroxenitos do Manto Litosférico Subcontinental do vulcão Agua Poca, Terreno Cuyania, Argentina. *Pesquisas en Geociencias*, 37, 143–167.

Kay, S.M., Ardolino, A.A., Gorrington, M.L., Ramos, V.A., 2007. The Somuncura large igneous province in Patagonia: Interaction of a transient mantle thermal anomaly with a subducting slab. *J. Petrol.* 48, 43–77.

Kay, S.M., Jones, H.A., Kay, R.W., 2013. Origin of Tertiary to recent EM-and subduction-like chemical and isotopic signatures in Auca Mahuida region (37–38 S) and other Patagonian plateau lavas. *Contrib. Mineral. Petrol.* 166 (1), 165–192.

Kelemen, P.B., 1990. Reaction between ultramafic rock and fractionating basaltic magma I. Phase relations, the origin of calc-alkaline magma series, and the formation of discordant dunite. *Journal of Petrology*, 31, 51–98. <https://doi.org/10.1093/petrology/31.1.51>

Kempton, P., Hawkesworth, C., Lopez-Escobar, L., Pearson, D.G., Ware, A.J., 1999. Spinel ± garnet lherzolite xenoliths from Pali Aike: part 2. Trace element and isotopic evidence bearing on the evolution of lithospheric mantle beneath southern Patagonia. *7th Int. Kimberlite Conf. Dawson Volume*. 1: 415–428.

Jing, J.-J., Su, B.-X., Xia, Y., Zhang, H.F., Uysal, I., Chen, C., Lin, W., Chu, Y., Saka, S., 2019. Reactive origin of mantle harzburgite: Evidence from orthopyroxene-spinel association. *Lithos*, 342–343, 175–186.

Labudía, C., 1994. Petrología y geoquímica de xenolitos lherzolíticos de las localidades de Lenzaniyeu y Paso de Indios – Comarca Nordpatagónica. II Jornadas de Mineralogía, Petrografía y Metalogénesis de Rocas Ultrabásicas, Universidad Nacional de La Plata, La Plata, Argentina. 3: 523–532.

Laurora, A., Mazzucchelli, M., Rivalenti, G., Vannucci, R., Zanetti, A., Barbieri, M.A., Cingolani, C.A., 2001. Metasomatism and melting in carbonated peridotite xenoliths from the mantle wedge: the Gobernador Gregores case (southern Patagonia). *Journal of Petrology*, 42, 69–87. <https://doi.org/10.1093/petrology/42.1.69>

Liu, S., Tommasi, A., Vauchez, A., Mazzucchelli, M., 2019a. Deformation, Annealing, Melt-Rock Interaction, and Seismic Properties of an Old Domain of the Equatorial Atlantic Lithospheric Mantle. *Tectonics*, 38, 1164–1188. <https://doi.org/10.1029/2018TC005373>

Liu, S., Tommasi, A., Vauchez, A., Mazzucchelli, M., 2019b. Crust-mantle coupling during continental convergence and break-up: Constraints from peridotite xenoliths from the Borborema Province, northeast Brazil. *Tectonophysics*, 766, 249–269. <https://doi.org/10.1016/j.tecto.2019.05.017>

Mazzucchelli, M., Rivalenti, G., Piccirillo, E.M., Girardi, V.A.V., Civetta, L., Petrini, L., 1995. Petrology of the Proterozoic mafic dyke swarms of Uruguay and constraints on their mantle source composition. *Precambrian Research*, 74/3, 177–194.

Formatted: Spanish (Mexico)

Formatted: Spanish (Mexico)

Formatted: English (United States)

Formatted: English (United States)

Formatted: English (United States)



Mazzucchelli, M., Rivalenti, G., Brunelli, D., Zanetti, A., Boari, E., 2009. Formation of Highly Refractory Dunite by Focused Percolation of Pyroxenite-Derived Melt in the Balmuccia Peridotite Massif (Italy). *Journal of Petrology*, 50, 1205-1233. <https://doi.org/10.1093/petrology/egn053>

Mazzucchelli, M., Cipriani, A., Hémond, C., Zanetti, A., Bertotto, G.W., Cingolani, C.A., 2016. Origin of the DUPAL anomaly in mantle xenoliths of Patagonia (Argentina) and geodynamic consequences. *Lithos*, 248-251, 257-271. <https://doi.org/10.1016/j.lithos.2016.01.010>

McDonough, W.F., Sun, S., 1995. The composition of the Earth. *Chemical Geology*, 120, 223-253. [https://doi.org/10.1016/0009-2541\(94\)00140-4](https://doi.org/10.1016/0009-2541(94)00140-4)

Melchiorre, M., Coltorti, M., Gregoire, M., Benoit, M., 2015. Refertilization process in the Patagonian subcontinental lithospheric mantle of Estancia Sol de Mayo (Argentina). *Tectonophysics*, 650, 124-143. [10.1016/j.tecto.2015.02.015](https://doi.org/10.1016/j.tecto.2015.02.015)

Melchiorre, M., Faccini, B., Grégoire, M., Benoit, M., Casetta, F., Coltorti, M., 2020. Melting and metasomatism/refertilisation processes in the Patagonian sub-continental lithospheric mantle: A review. *Lithos*, 354-355, 105324. <https://doi.org/10.1016/j.lithos.2019.105324>

Mercier, J.-C.C., 1980. Single-pyroxene thermobarometry. *Tectonophysics*, 70, 1-37. [https://doi.org/10.1016/0040-1951\(80\)90019-0](https://doi.org/10.1016/0040-1951(80)90019-0)

Mundl, A., Ntaflos, T., Ackerman, L., Bizimis, M., Bjerg, A., 2015. Geochemical and Os–Hf–Nd–Sr Isotopic Characterization of North Patagonian Mantle Xenoliths: Implications for Extensive Melt Extraction and Percolation Processes. *Journal of Petrology*. *Journal of Petrology*, 57, 685-715. <https://doi.org/10.1093/petrology/egv048>

Muñoz, J., Troncoso, R., Duhart, P., Crignola, P., Farmer, L., Stern, C.R., 2000. The relation of the mid-Tertiary coastal magmatic belt in south-central Chile to the late Oligocene increase in plate convergence rate. *Rev. Geol. Chile*, 27, 177–203.

Ntaflos, Th., Bjerg, E.A., 2006. Garnet-bearing xenoliths from Prahuaníyeu N-Patagonia: a LA-ICP-MS study. 16<sup>th</sup> Annual VM Goldschmidt Conference August-September 2006, *Geochimica et Cosmochimica Acta*, 70 (18), Supplement 1, Page A450.

Ntaflos, Th., Bjerg, E.A., Labudía, C.H., Thöni, M., Frisicale, C., Günther, M., 2001. Garnet-bearing xenoliths: evidence of plume activity in northern Patagonia. *Proceedings of the 11th Annual Goldschmidt Conference abstract #3126*.

Ntaflos, Th., Bjerg, E.A., Labudía, C.H., Kurat, G., 2007. Depleted lithosphere from the mantle wedge beneath Tres Lagos, southern Patagonia, Argentina. *Lithos*, 94, 46–65. <https://doi.org/10.1016/j.lithos.2006.06.011>

Ozawa, K., 2001. Mass balance equations for open magmatic systems: Trace element behavior and its application to open system melting in the upper mantle. *Journal of Geophysical Research*, 106, 13407-13434. <https://doi.org/10.1029/2001JB900001>

Ozawa, K., Shimizu, N., 1995. Open-system melting in the upper mantle: Constraints from the Hayachine–Miyamori ophiolite, northeastern Japan. *Journal of Geophysical Research*, 100, 22315-22335. <https://doi.org/10.1029/95JB01967>

Ponce, A., Bertotto, G., Zanetti, A., Brunelli, D., Giovanardi, T., Aragón, E., Bernardi, M., Hémond, C. y Mazzucchelli, M. 2015. Short-scale variability of the SCLM beneath the extra-Andean back arc (Paso de Indios, Argentina): Evidence from spinel-facies mantle xenoliths. *Open Geosciences*, 7, 362-385. <https://doi.org/10.1515/geo-2015-0023>

Ramos, V., 1999. Las Provincias Geológicas del Territorio Argentino. In: Haller, M.J. (Ed.), *Geología Argentina*. Instituto de Geología y Recursos Minerales, Anales 29, Buenos Aires, pp. 41-96.



888 Rivalenti, G., Mazzucchelli, M., Molesini, M., Petrini, R., Girardi, V.A.V., Bossi, J.,  
889 Campal, N., 1995. Petrology of late proterozoic mafic dikes in the Nico Perez region,  
890 central Uruguay. *Mineralogy and Petrology*, 55, 239-263. 10.1007/BF01165120

891 Rivalenti, G., Mazzucchelli, M., Laurora, A., Ciuffi, S., Zanetti, A., Vannucci, R., Cingolani,  
892 C.A., 2004a. The back arc mantle lithosphere in Patagonia, South America. *Journal of*  
893 *South American Earth Sciences*, 17, 121-152.  
894 <https://doi.org/10.1016/j.jsames.2004.05.009>

895 Rivalenti, G., Zanetti, A., Mazzucchelli, M., Vannucci, R., Cingolani, C.A., 2004b. Equivocal  
896 carbonatite markers in the mantle xenoliths of the Patagonia backarc: the Gobernador  
897 Gregores case (Santa Cruz Province, Argentina). *Contributions to Mineralogy and*  
898 *Petrology*, 147, 647-670. <https://doi.org/10.1007/s00410-004-0582-2>

899 Rivalenti, G., Mazzucchelli, M., Zanetti, A., Vannucci, R., Bollinger, C., Hémond, C.,  
900 Bertotto, G.W., 2007a. Xenoliths from Cerro de los Chenques (Patagonia): An example  
901 of slab-related metasomatism in the backarc lithospheric mantle. *Lithos*, 99, 45-67.  
902 <https://doi.org/10.1016/j.lithos.2007.05.012>

903 Rivalenti, G., Zanetti, A., Girardi, V.A.V., Mazzucchelli, M., Tassinari, C.C.G., Bertotto,  
904 G.W., 2007b. The effect of the Fernando de Noronha plume on the mantle lithosphere in  
905 north-eastern Brazil. *Lithos*, 94, 111-131. 10.1016/j.lithos.2006.06.012

906 Roverato, M., Giordano, D., Giovanardi, T., Juliani, C., Polo, L., 2019. The 2.0–1.88 Ga  
907 Paleoproterozoic evolution of the southern Amazonian Craton (Brazil): an interpretation  
908 inferred by lithofaciological, geochemical and geochronological data. *Gondwana*  
909 *Research*, 70, 1-24. <https://doi.org/10.1016/j.gr.2018.12.005>

910 Schilling, M.E., Carlson, R.W., Conceição, R.V., Dantas, C., Bertotto, G.W., Koester, E.,  
911 2008. Re–Os isotope constraints on subcontinental lithospheric mantle evolution of  
912 southern South America. *Earth and Planetary Science Letters*, 268, 89-101.  
913 doi:10.1016/j.epsl.2008.01.005.

914 Schulze, D.J., 2001. Origins of chromian and aluminous spinel macrocrysts from kimberlites  
915 in southern Africa. *Canadian Mineralogist* 39 (2), 361-376. Silva Nieto, D.G., 2005.  
916 Descripción geológica de la Hoja 4369-III, Paso de Indios, Provincia del Chubut. Servicio  
917 Geológico Minero Argentino, Boletín N° 267, Buenos Aires.

918 Seyler, M., Lorand, J. P., Dick, H. J., & Drouin, M. (2007). Pervasive melt percolation  
919 reactions in ultra-depleted refractory harzburgites at the Mid-Atlantic Ridge, 15° 20' N:  
920 ODP Hole 1274A. *Contributions to Mineralogy and Petrology*, 153(3), 303.

921 Seyler, M., & Brunelli, D. (2018). Sodium-chromium covariation in residual clinopyroxenes  
922 from abyssal peridotites sampled in the 43°–46° E region of the Southwest Indian  
923 Ridge. *Lithos*, 302, 142-157.

924 Skewes, M.A., Stern, C.R., 1979. Petrology and geochemistry of alkali basalts and  
925 ultramafic inclusions from the Pali-Aike volcanic field in southern Chile and the origin  
926 of the Patagonian plateau lavas. *Journal of Volcanology and Geothermal Research* 6, 3-  
927 25.

928 Stern, C.R., Kilian, R., 1996. Role of the subducted slab, mantle wedge and continental crust  
929 in the generation of adakites from the Andean Austral Volcanic Zone. *Contributions to*  
930 *Mineralogy and Petrology*, 123, 263-281. doi:10.1007/s004100050155

931 Stern, C.R., Frey, F.A., Futa, K., Zartman, R.E., Peng, Z., Kyser, K.T., 1990. Trace-element  
932 and Sr, Nd, Pb, and O isotopic composition of Pliocene and Quaternary alkali basalts of  
933 the Patagonian Plateau lavas of southernmost South America. *Contributions to*  
934 *Mineralogy and Petrology* 104, 294-308. <https://doi.org/10.1007/BF00321486>

935 Sun, S., McDonough, W.F., 1989. Chemical and isotopic systematics of oceanic basalts;  
936 implications for mantle composition and processes. En: *Magmatism in the Ocean Basins*

Formatted: English (United States)

Formatted: English (United States)

Formatted: English (United States)

- (Saunders, A. y Norry, M., eds.), Geological Society Special Publication 42, 313-345. <https://doi.org/10.1144/GSL.SP.1989.042.01.19>
- Taylor, W.R., 1998. An experimental test of some geothermometer and geobarometer formulations for upper mantle peridotites with application to the thermobarometry of fertile lherzolite and garnet websterite. *Neues Jb. Miner. Abh.* 172: 381-408. <https://doi.org/10.1127/njma/172/1998/381>
- Vannucci, R., Zanetti, A., Kempton, P.D., Ciuffi, S., Mazzucchelli, M., Cingolani, C.A., 2002. The chemical history of young lithospheric mantle in a backarc region: the spinel±garnet peridotite xenoliths from Pali Aike (south Patagonia). *Decimoquinto Congreso Geológico Argentino, El Calafate, Argentina. Actas* 3, 71-74.
- Warren, J.M., 2016. Global variations in abyssal peridotite compositions. *Lithos*, 248-251, 193-219.
- Zaffarana, C., Tommasi, A., Vauchez, A., Grégoire, M. 2014. Microstructures and seismic properties of south Patagonian mantle xenoliths ( Gobernador Gregores and Pali Aike ). *Tectonophysics*, 621, 175-197. <https://doi.org/10.1016/j.tecto.2014.02.017>
- Zanetti, A., Giovanardi, T., Langone, A., Tiepolo, M., Wu, F.-Y., Dallai, L., Mazzucchelli, M., 2016. Origin and age of zircon-bearing chromitite layers from the Finero phlogopite peridotite (Ivrea–Verbano Zone, Western Alps) and geodynamic consequences. *Lithos*, 262, 58–74. <http://dx.doi.org/10.1016/j.lithos.2016.06.015>

## Figure Captions

Fig. 1. Geologic map of the study area and location of Chenque, León and Matilde hills, modified after Ponce et al. (2015). The three localities are framed in red.

Fig. 2. A: Modal composition of the studied PDI xenoliths. Star (PM) primitive mantle after Warren (2016). The grey field represents the variation of anhydrous Patagonian xenoliths from Rivalenti et al. (2004a) and Bjerg et al. (2005). B: pyroxenes vs olivine contents of PDI lherzolite xenoliths. B: pyroxenes vs olivine contents of PDI harzburgite xenoliths. Filled symbols are new samples from this work, white-filled symbols are samples from Ponce et al. (2015). PM values are from Warren (2016).

Fig. 3. Photomicrographs of PDI mantle xenoliths under cross-polarized light. A) Porphyroclastic texture of sample Q77. B) Transitional coarse to porphyroclastic texture of harzburgite MH. C) Transitional coarse to porphyroclastic texture of harzburgite L82a and D) mosaic-porphyroclastic texture of lherzolite Q65. E) Olivine relict within orthopyroxene in harzburgite M55. F) Interstitial secondary orthopyroxene growing at olivine borders in harzburgite Q101. G) Contact of the xenolith with the host basalt and development of a reaction corona (harzburgite sample M67). H) secondary orthopyroxene engulfing a primary olivine (lherzolite M53). I) SEM image of basalt-xenolith contact and reaction zone in lherzolite L91. L) spongy clinopyroxene and associated glass veins in harzburgite L82a. Ol: olivine; opx: orthopyroxene; cpx: clinopyroxene; spl: spinel.

Fig. 4. (A) NiO vs Mg# in olivine from the PDI area; (B) Cr# vs Mg# of spinels and fields of the spinel classification of Schilze (2001); Al<sub>2</sub>O<sub>3</sub> vs. Mg# for orthopyroxenes (C) and clinopyroxenes (D). Grey fields are the compositional variations determined by Melchiorre et al. (2020) and references therein for peridotitic and pyroxenitic xenoliths of North Patagonia.

Formatted: English (United States)

Fig. 5. C1 chondrite (Anders and Grevesse, 1988) normalized REE elements patterns and primitive mantle (PM, Sun and McDonough 1989) normalized spiderdiagrams of clinopyroxenes. A) group I: LREE depleted patterns; B) group II: LREE enriched patterns; C) group III: “U” and “V”-shaped patterns; D) group IV: sinusoidal patterns and E) group V: flat patterns to weakly LREE enriched;. The pattern of a primitive mantle-cpx (solid black line) of Sun and McDonough (1989) and patterns (gray lines) after 1, 3, 5, 10, 15 and 20% of depletion by partial non-modal melting, are also shown. For comparison, data from PDI xenoliths from literature (Rivalenti et al., 2004a) are reported as dashed lines. Trace elements extended diagrams are reported with values normalized to the Primitive Mantle composition recalculated from Pyrolite (PM; McDonough and Sun, 1995).

Fig. 6. Pressure (GPa) vs. Temperature (°C). Temperatures were calculated with the Ca-inOpx geothermometer of Brey and Köhler (1990). L: lherzolite; H: harzburgite; W: websterite and olivine-websterite. Data from other Patagonian localities are reported for comparison: Prahuaníyeu is from Bjerg et al. (2009); Tres Lagos is from Mazzucchelli et al. (2016); Agua Poca is from Bertotto et al. (2013); Río Negro, Gobernador Gregores and Pali Aike are from Bjerg et al. (2005).

Fig. 7. A: modal clinopyroxene content vs spinel Cr# diagram. B: modal clinopyroxene content vs Yb in clinopyroxene normalized to the C1 chondrite (Anders and Grevesse, 1988). C: Mg# vs Na<sub>2</sub>O (wt.%) in clinopyroxene. D: Al<sub>2</sub>O<sub>3</sub> vs Cr<sub>2</sub>O<sub>3</sub> (wt.%) in clinopyroxene. E: Cr<sub>2</sub>O<sub>3</sub> vs Na<sub>2</sub>O (wt.%) in clinopyroxene. F: Forsterite (Fo) vs NiO (wt%) in olivine. Data from abyssal peridotite (Warren et al., 2016) and VEMA mantle rocks (Brunelli et al., 2006; Cipriani et al., 2009) are reported for comparison. Red arrows identify the fractional melting trend.

Fig. 8. Potential melts in equilibrium with PDI clinopyroxenes from A) Group I and B) Group V, normalized to the Primitive Mantle composition recalculated from Pyrolite (PM; McDonough and Sun, 1995). Melts are calculated using the clinopyroxene/melt partition coefficient of Ionov et al. (2002) for Group I and of Green et al. (2000) and Hauri et al. (1994) for Group V. Host basalts (Chenque, Matilde and León) from Alric (1996) are reported for comparison. The grey fields are: dark grey - arc basalts from the Patagonian region from Hickey et al. (1986) and D’Orazio et al. (2003); light grey - adakites from the Austral Volcanic Zone from Stern and Kilian (1996).

Fig. 9. Open-system model for the PDI xenoliths.

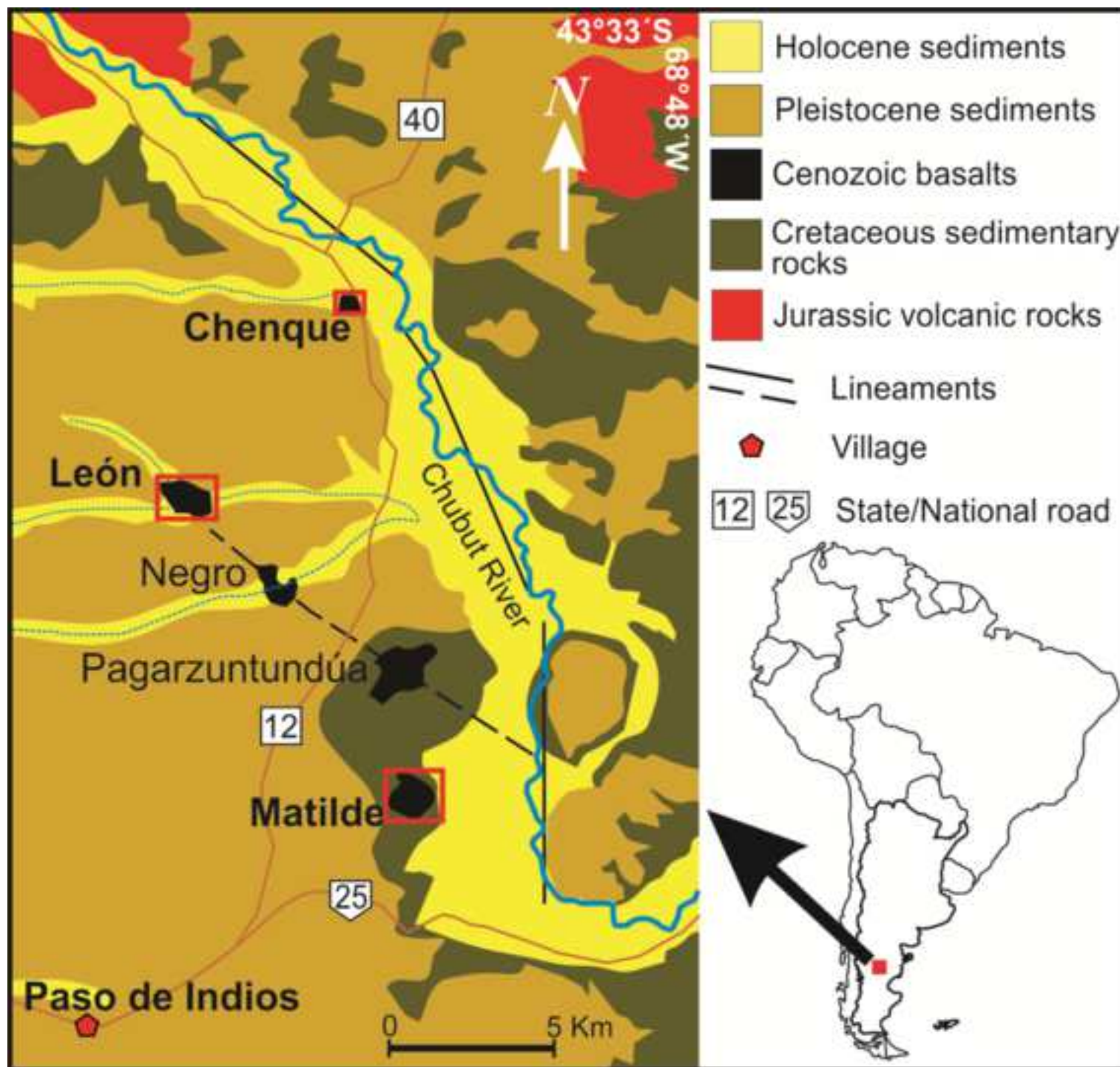
Fig. 10: Tectonic Model for the PDI mantle evolution during adakitic-like melt infiltration in a orthopyroxene-rich, clinopyroxene-poor mantle column. After the Cretaceous flat slab event different tectonic configurations were proposed to explain the alkaline features of the Paleocene-Eocene magmas, that are either the opening of a slab window (Iannelli et al. 2017; Fernandez Paz et al., 2018), or a pure a slab rollback of the Farallon plate (Muñoz et al., 2000; Echaurren et al., 2016, 2019), or a complete detachment of the Aluk plate and the formation of a transform margin (Aragón et al., 2011; 2015). In the figure, for simplicity, we used for the asthenospheric mantle ascent two possibilities: with subduction and opening of a slab window (Fernández Paz et al., 2018) or without subduction (Aragón et al. 2011, 2015).

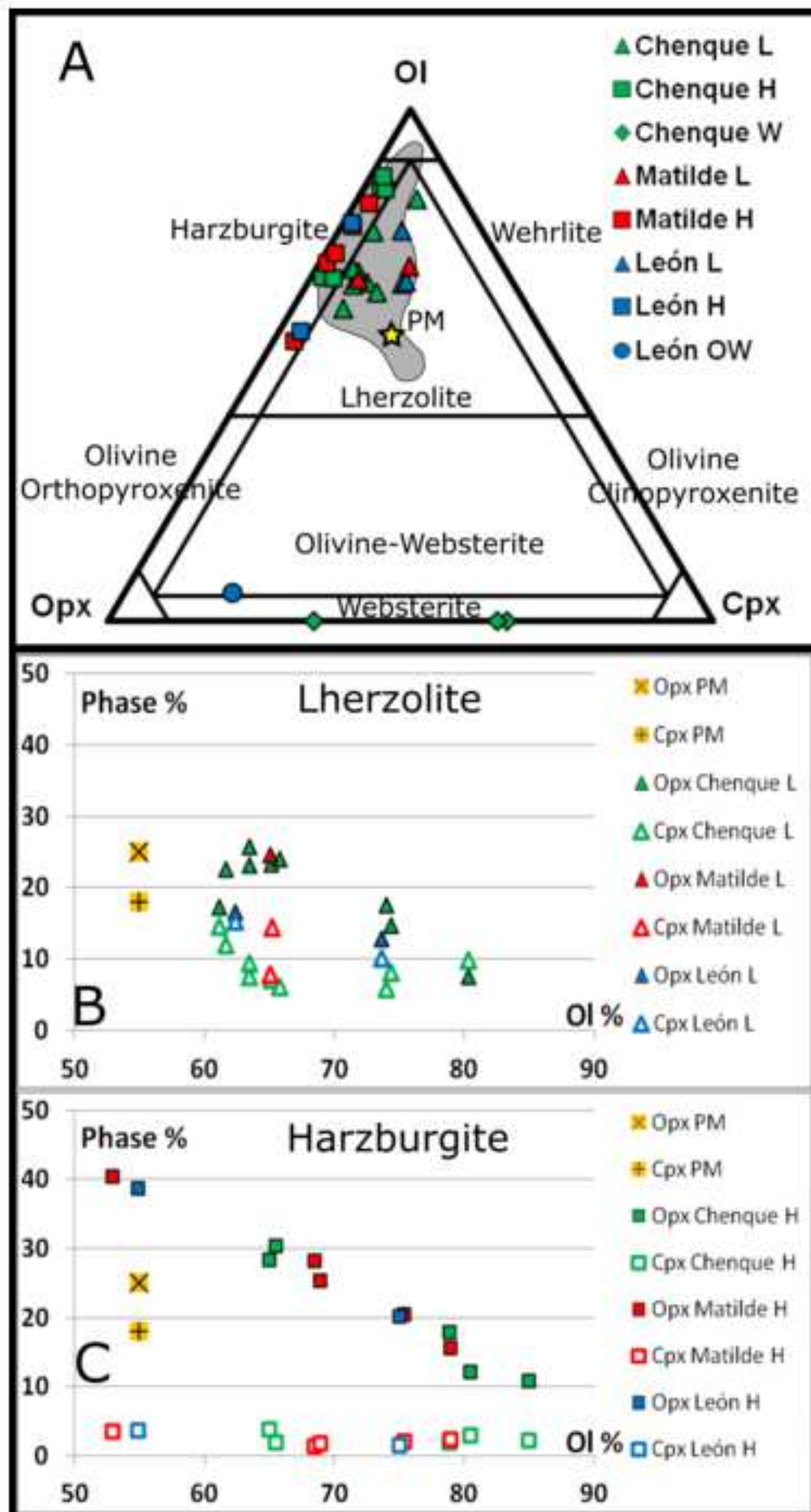
# Table

Table 1. Modal composition of the PDI xenoliths. Q are from Chenque, M are from Matilde and L are from León. H: harzburgite; L: lherzolite; W: websterite and OW: olivine-websterite.

1037  
1038 Table 2. Average olivine major element compositions. L: lherzolite; H: harzburgite; SD is  
1039 standard deviation. b.d.l.: below detection limit. Values are wt.%.  
1040  
1041 Table 3. Average spinel major element compositions. L: lherzolite; H: harzburgite; OW:  
1042 olivine websterite; SD is standard deviation. b.d.l.: below detection limit. Values are wt.%.  
1043  
1044 Table 4. Average orthopyroxene major element compositions. L: lherzolite; H: harzburgite;  
1045 OW: olivine websterite; W: websterite; SD is standard deviation. b.d.l.: below detection  
1046 limit. Values are wt.%.  
1047  
1048 Table 5. Average clinopyroxene major element compositions. L: lherzolite; H: harzburgite;  
1049 OW: olivine websterite; W: websterite; SD is standard deviation. b.d.l.: below detection  
1050 limit. Values are wt.%.  
1051  
1052 Table 6. Average clinopyroxene trace element composition. L: lherzolite; H: harzburgite;  
1053 OW: olivine websterite; W: websterite; SD is standard deviation. b.d.l.: below detection  
1054 limit. Values are in ppm.  
1055  
1056 Table 7. Temperature (T-°C) and pressure (P-GPa) estimations from PDI xenoliths after data  
1057 collected by Ponce et al. (2015) and this work. Type of lithologies is as follow: L: lherzolite;  
1058 H: harzburgite; OW: olivine websterite; W: websterite. Geothermometer and geobarometer  
1059 references: BKN = two-pyroxene thermometer (Brey and Köhler, 1990); Ca-Opx = Ca in  
1060 orthopyroxene thermometer (Brey and Köhler, 1990); TA98 = two-pyroxene thermometer  
1061 (Taylor, 1998); PMc = clinopyroxene barometer (Mercier, 1980). SD is standard deviation.  
1062  
1063  
1064  
1065  
1066

Figure 1







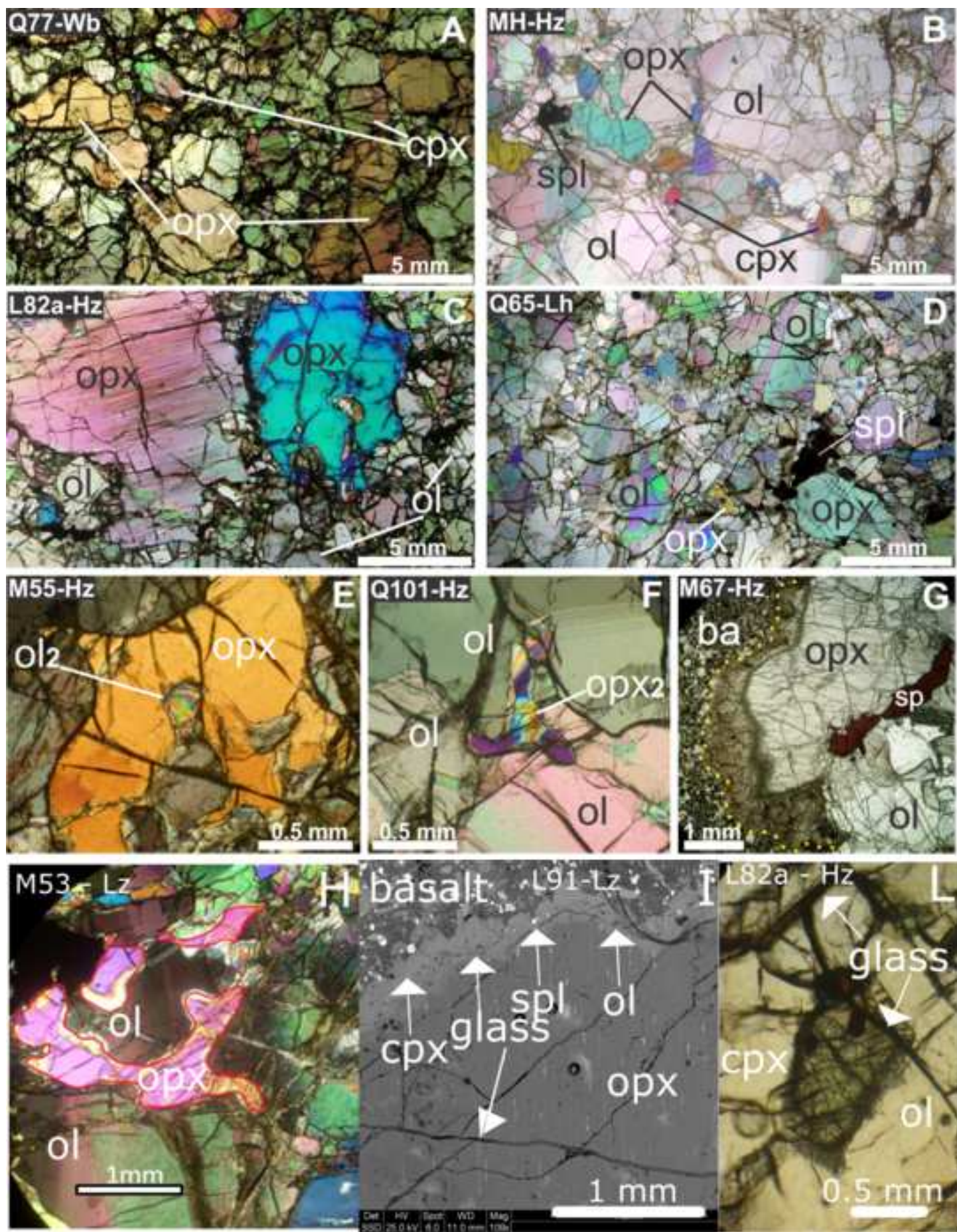
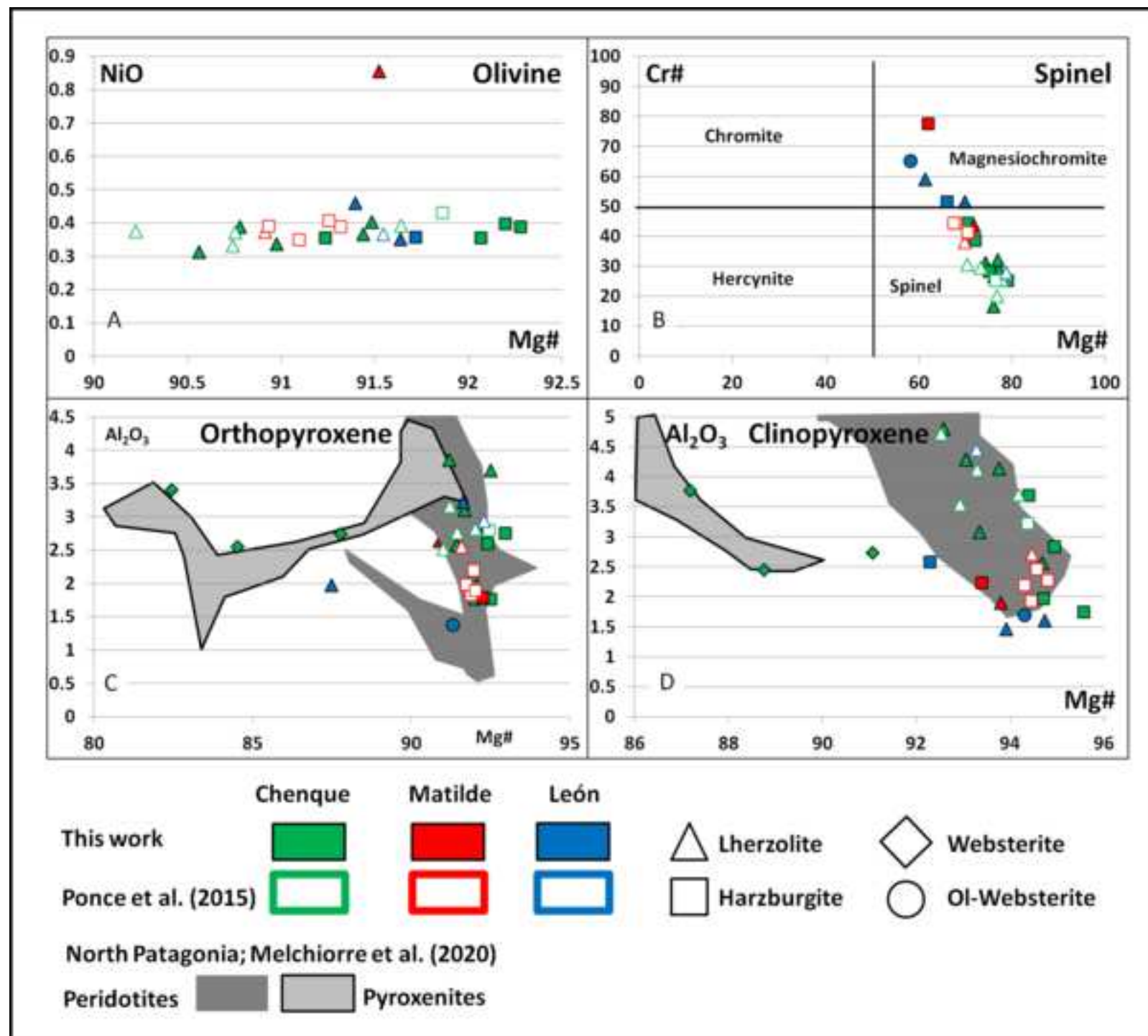




Figure 4

[Click here to access/download;Figure;Fig 4\\_rev.png](#)





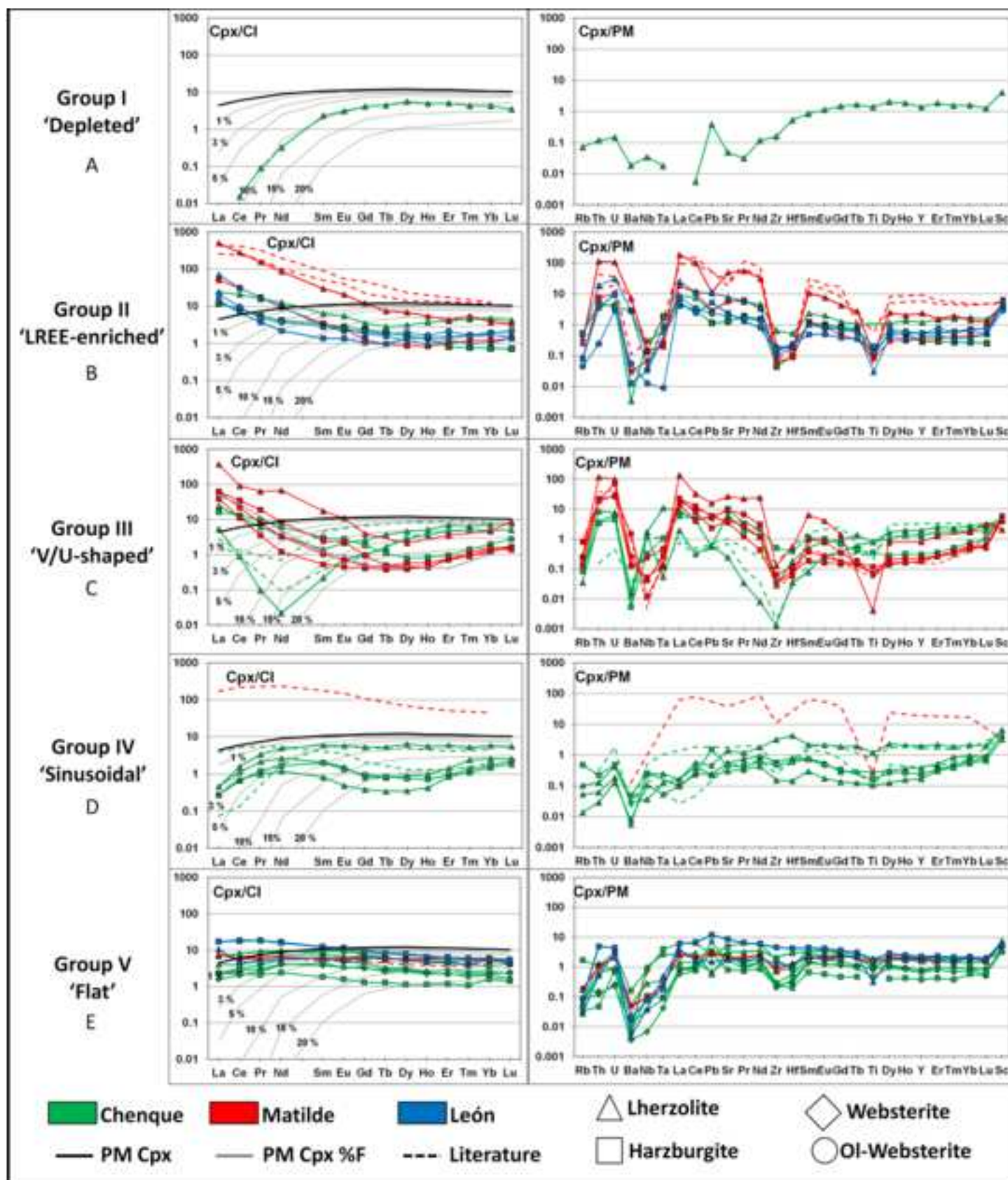
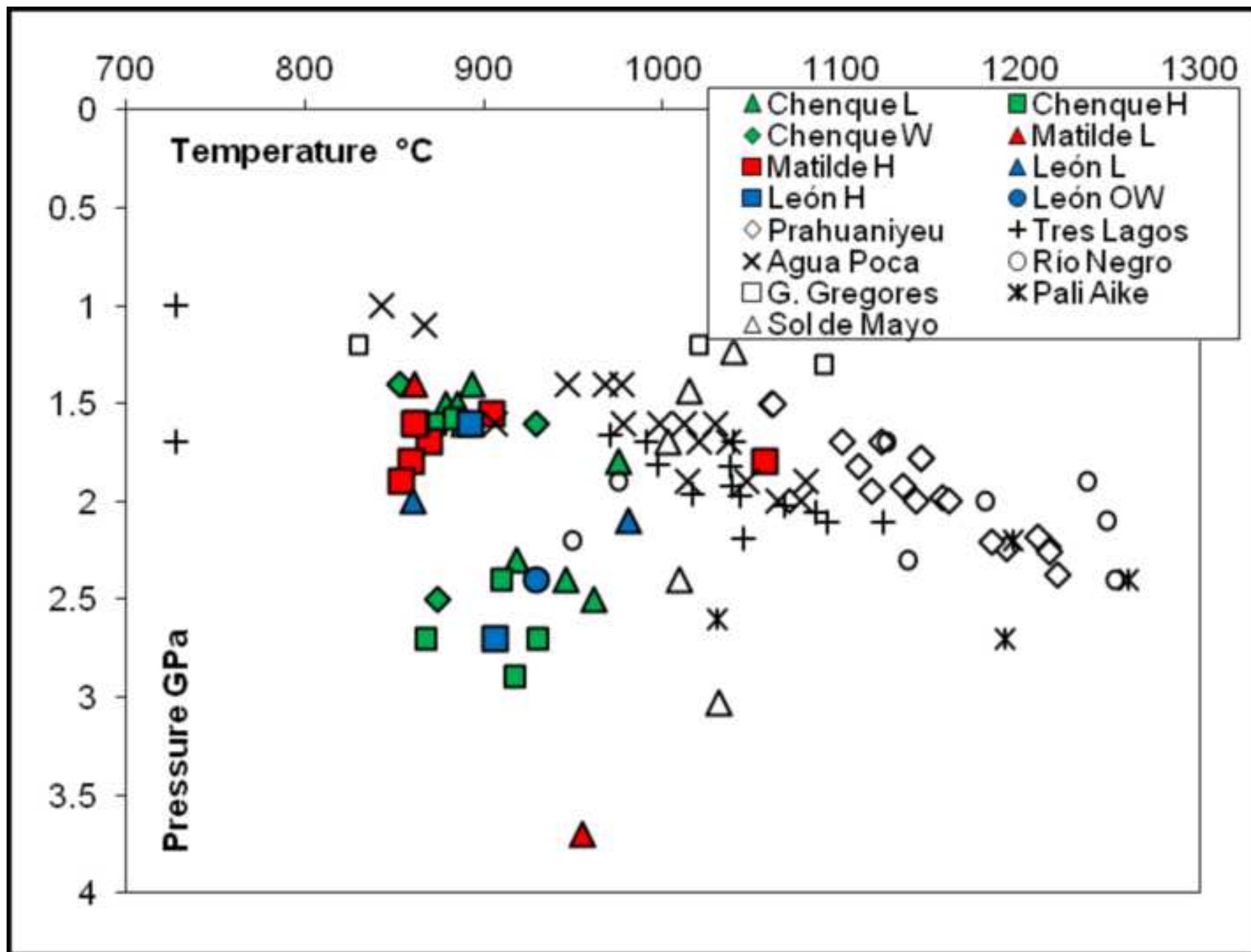


Figure 6

[Click here to access/download;Figure;Fig 6\\_rev2.png](#)

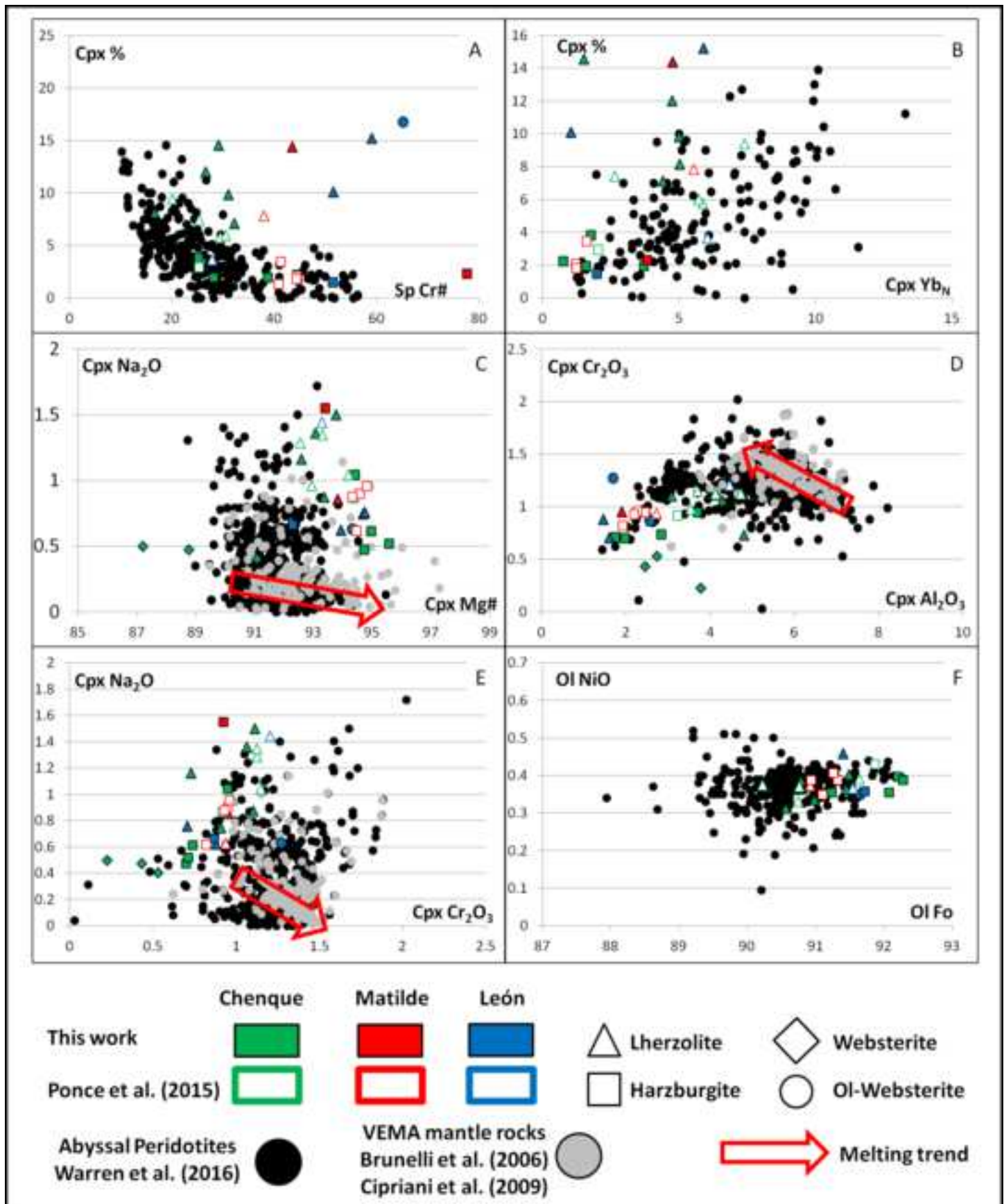




Figure 8

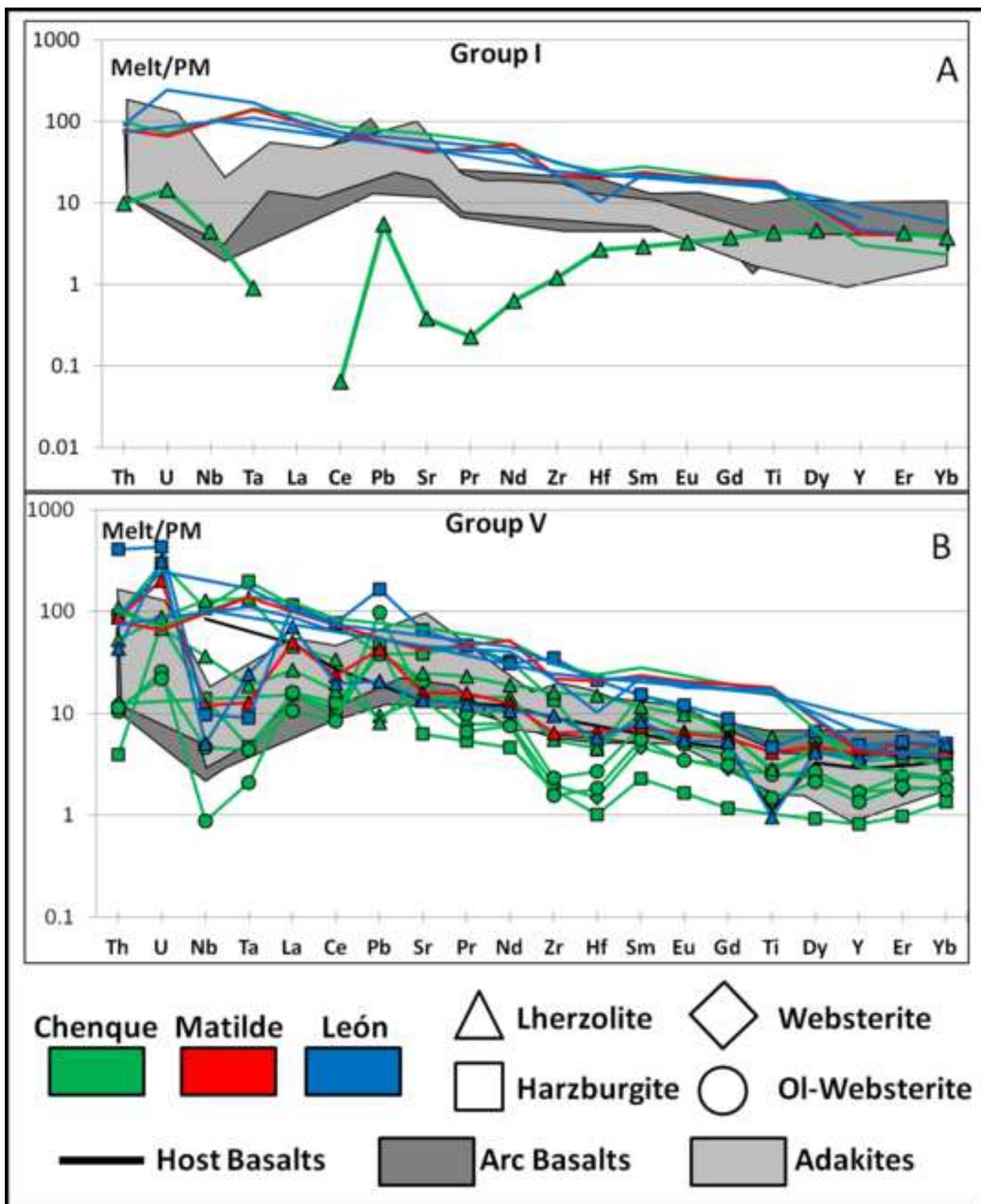
[Click here to access/download;Figure;Fig 8\\_rev.png](#)

Figure 9

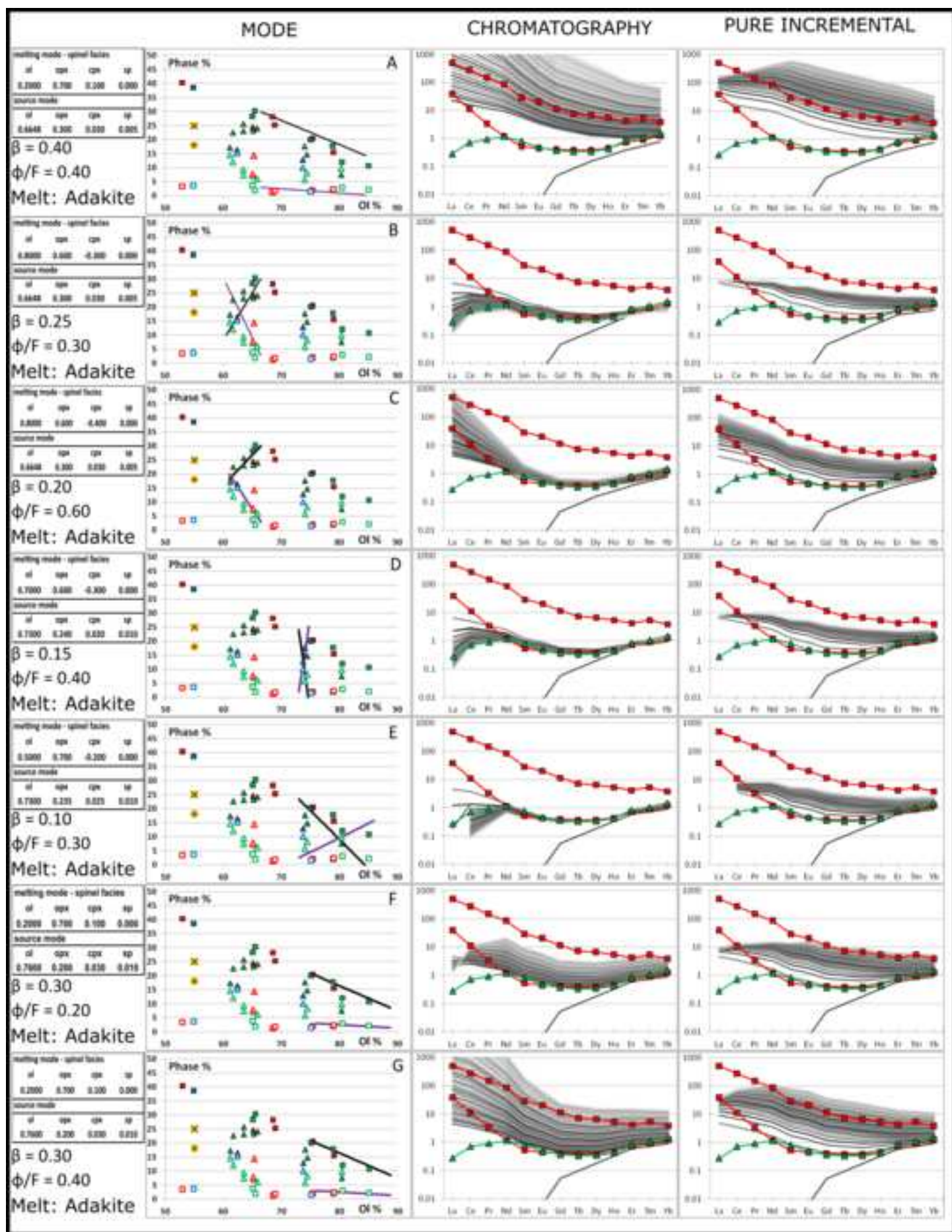
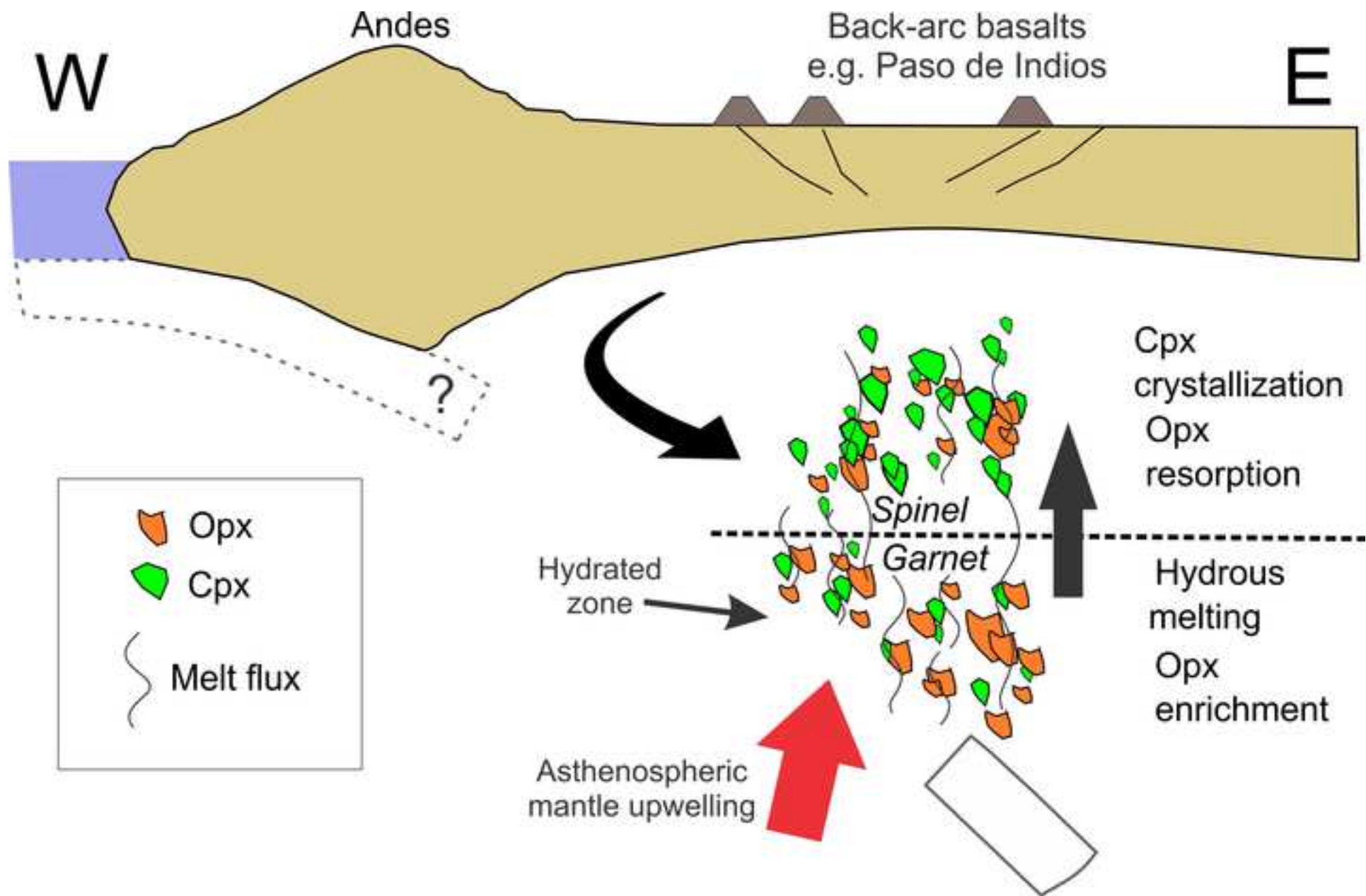
[Click here to access/download;Figure;Fig 9.png](#)



Figure 10







Click here to access/download  
**Table**  
Table 2\_rev2.docx





Click here to access/download  
**Table**  
Table 3\_rev2.docx



Click here to access/download  
**Table**  
Table 4\_rev2.docx



Click here to access/download  
**Table**  
Table 5\_rev2.docx



Click here to access/download  
**Table**  
Table 6\_rev2.docx



Click here to access/download  
**Table**  
Table 7\_rev2.docx



[Click here to access/download](#)

**Table**

Supplementary Material 1\_rev2.docx





[Click here to access/download](#)

**Table**

[Supplementary Material 2\\_rev2.xlsx](#)







[Click here to access/download](#)

**Table**

[Supplementary Material 3\\_rev2.xlsx](#)





[Click here to access/download](#)

**Table**

[Supplementary Material 4\\_rev2.docx](#)

